A critical appraisal of polymer–clay nanocomposites

Biqiong Chen,[a] Julian R. G. Evans,*[b] H. Christopher Greenwell,[c] Pascal Boulet,[d] Peter V. Coveney,[e] Allen A. Bowden[f] and Andrew Whiting[c]

Received 13th November 2007
First published as an Advance Article on the web 13th December 2007
DOI: 10.1039/b702653f

The surge of interest in and scientific publications on the structure and properties of nanocomposites has made it rather difficult for the novice to comprehend the physical structure of these new materials and the relationship between their properties and those of the conventional range of composite materials. Some of the questions that arise are: How should the reinforcement volume fraction be calculated? How can the clay gallery contents be assessed? How can the ratio of intercalate to exfoliate be found? Does polymerization occur in the clay galleries? How is the crystallinity of semi-crystalline polymers affected by intercalation? What role do the mobilities of adsorbed molecules and clay platelets have? How much information can conventional X-ray diffraction offer? What is the thermodynamic driving force for intercalation and exfoliation? What is the elastic modulus of clay platelets? The growth of computer simulation techniques applied to clay materials has been rapid, with insight gained into the structure, dynamics and reactivity of polymer–clay systems. However these techniques operate on the basis of approximations, which may not be clear to the non-specialist. This *critical review* attempts to assess these issues from the viewpoint of traditional composites thereby embedding these new materials in a wider context to which conventional composite theory can be applied. (210 references)

[a]*Department of Materials, Queen Mary, University of London, Mile End Road, London, UK E1 4NS*
[b]*Department of Chemistry, University College London, Christopher Ingold Laboratories, 20 Gordon Street, London, UK WC1H 0AJ. E-mail: j.r.g.evans@ucl.ac.uk; Tel: 0044 20 7679 4689*
[c]*Department of Chemistry, Durham University, South Road, Durham, UK DH1 3LE*
[d]*MADIREL - MAtériaux DIvisés, Revêtements, ELectrocéramiques UMR 6121, Université de Provence - Aix-Marseille I, Centre de Saint-Jérôme, 13397, MARSEILLE Cedex 20, France*
[e]*Centre for Computational Science, Department of Chemistry, University College of London, 20 Gordon Street, London, UK WC1H OAJ*
[f]*Department of Chemistry, The Open University, Robert Hooke Building, Walton Hall, Milton Keynes, UK MK7 6AA*

1. Introduction

This review focuses on polymer–clay nanocomposites for which the number of published scientific papers has grown dramatically from a few papers in the early 1990s to about 770 in 2006. It is a salutary lesson that interest in polymer–clay nanocomposites did not emerge from the far-sightedness of the academic community but from a brave commercial initiative.[1] These studies reflect a response to that initiative that has grown in opposition to the earlier prevailing wisdom that research into clays was largely complete and little new materials science was to be found therein. Some of that literature is difficult to interpret because the characterization

Biqiong Chen

Dr Biqiong Chen studied for her BSc and MSc degrees in Polymer Science and Engineering in China. She started her research in polymer–clay nanocomposites in 2001 under the supervision of Prof. J. R. G. Evans at Queen Mary, University of London. After gaining her PhD, she spent three more years with Prof. Evans studying fundamental aspects and applications of polymer–clay nanocomposites.

H. Christopher Greenwell

Dr Chris Greenwell is the Addison Wheeler Fellow at Durham University. He is also an Honorary Research Fellow at the Centre for Computational Science, University College London. Greenwell studied for his BSc at the University of Wales Bangor, where he was awarded the Evan Roberts prize and the Peboc medal in chemistry and the Dr John Roberts Jones University prize, prior to undertaking his PhD (2003) in the Materials Chemistry Group, Cambridge under the supervision of Prof. W. Jones. His research interests focus on the structure and behaviour of layered solids.

of materials was incomplete or ambiguous. Thus the relationship between permeation or mechanical properties and volume fraction is poorly understood because it is not clear how the actual volume fraction of reinforcement, a principal parameter in composite materials, should be calculated. Evidence for intercalation is complicated by the fact that swelling effects detectable by X-ray diffraction (XRD) might result from impurities or adsorption at the edge of tactoids. Since XRD cannot detect exfoliation, a partially exfoliated composite can pass for an intercalated composite.

In general, the properties of polymers are largely improved and new unexpected features may appear after the addition of clay. As a result, some nanocomposites have been used as automobile components, packaging materials, construction materials, flame retardants, protective films and so on. Applications for most nanocomposites can be divided into two broad categories that relate to engineering or barrier properties, with electrical properties and biodegradability featuring in some cases. The pioneering use of a nylon–clay nanocomposite was in Toyota cars in 1989.[1] Unlike conventional composites, they offered substantial increases in tensile strength, tensile modulus and storage modulus, with little or no loss in impact resistance. Impact strength is not universally reported for polymer–clay nanocomposites, which is surprising in view of the importance of this property for design and use. Some polymers retain impact strength when clay is dispersed[1,2] but for others toughness is reduced.[3,4] Improvements in barrier properties, such as solvent, moisture or gas permeation and flame resistance, are normally gained without loss of optical clarity in these composites at levels of clay addition of 1–5 vol%.[5]

Polymers and clays do not always form nanocomposites and modification of either the clay or the polymer is sometimes necessary. Such modifications can change a conventional composite to a nanocomposite or make an intercalated nanocomposite exfoliate. For example, the modification of montmorillonite (MMT) by quaternary ammonium compounds changes a conventional composite of poly(ε-caprolactone) (PCL)–montmorillonite to an intercalated nanocomposite.[6,7] Clays are also susceptible to modification by cation exchange (*vide infra*). The treatment of polyethylene (PE) with maleic anhydride allows it to form an exfoliated nanocomposite[8] by changing its polarity whereas unmodified PE produces a conventional composite with clay, in which the clay particles are simply interspersed with the layered structure intact within the polymer.

This review examines the relationship between nanocomposites and conventional composites. It notes that the surge of interest in any subject with the prefix "nano" tends to create a separate identity for the subject matter, particularly in the mind of the novice, that may not be fully justified by observation and experiment.

2. Definitions of terms

Composite materials can be defined as a combination of two or more materials which are physically distinct, readily distinguished by microscopy, dispersed in a controlled way to achieve optimum properties and in which the properties are superior to those of the individual components.[9] The International Union of Pure and Applied Chemistry specification[10] defines a composite as "A multicomponent material comprising multiple different (non-gaseous) phase domains in which at least one type of phase domain is a continuous phase". It also defines nanocomposites as composite materials "in which at least one of the phases has at least one dimension of the order of nanometres". In this class of materials are to be found dispersions of nanoparticles in a continuous matrix, dispersions of nanometre fibres, principally carbon nanotubes in a matrix, and the intercalation and/or exfoliation of smectite minerals within a continuous phase. Polymer–clay nanocomposites fall in the last category and owe their prominence largely to the rapid commercial exploitation of nylon–clay composites for engine components by Toyota automotive corporation.

Polymer–clay composites based on layered silicates can be classified into three types depending on the extent of separation of the silicate layers: conventional composites, intercalated nanocomposites and exfoliated nanocomposites,[5] shown schematically in Fig. 1. The distance between a plane in the unit layer and the corresponding plane in the next unit layer is defined as the basal plane spacing, d_{001}. If the polymer does not enter the galleries, d_{001} of clay remains unchanged

Allen Bowden

Allen Bowden obtained his PhD at SUNY at Buffalo in 1999 under the supervision of Prof. J. D. Atwood. This was followed by a two year postdoctoral stay at Dartmouth College with Prof. R. P. Hughes. He then returned to the UK for three further years of postdoctoral research at The University of Durham with Dr A. Whiting studying polymer–clay nanocomposites in collaboration with Prof J. R. G. Evans and Prof. P. V. Coveney. He is currently responsible for the NMR, Mössbauer and XRD machines at the Open University in Milton Keynes.

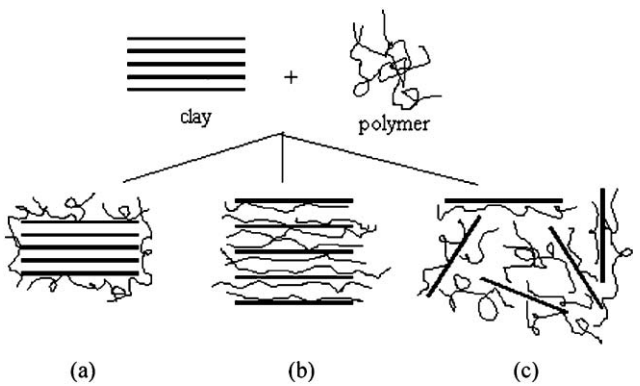

Fig. 1 Schematic representation of different types of composite (a) conventional composite; (b) intercalated nanocomposite; and (c) exfoliated nanocomposite.

and the composite is "conventional". If an organic species enters the galleries causing an increase in d_{001}, but the clay layers remain stacked, the composite is 'intercalated'. The value of d_{001} is a witness to the fact that organic matter has swollen the clay but it is silent on the amount of intercalated matter, on the extent of partial exfoliation that may have accompanied this change and on the identity of the guest species in the galleries.

If the clay layers are completely pushed apart to create a disordered array, the composite is considered to be 'exfoliated'. For some authors,[5,11] a composite for which $d_{001} > 10$ nm, a spacing that cannot be determined by a conventional X-ray diffractometer, is designated as exfoliated. As a result, there are two types of exfoliation; ordered and disordered. Recently Ray *et al.* defined another type of nanocomposite within the set of 'intercalated nanocomposites', namely intercalated-and-flocculated nanocomposites which contain flocculated intercalated silicate layers due to the hydroxylated edge–edge interaction of the silicate layers.[12] In fact, most intercalated tactoids include both single stacks and several connected stacks of clay layers so the distinction between flocculation and intercalation rests on electron microscopic analysis of the structure. Moreover, the 'flocculation' could be attributed to the long molecular chains that intercalate into two or more clay galleries and play a bridging role.[13,14] Electron microscopy often shows that most nanocomposites are both intercalated and exfoliated[15] but this is not readily deduced from X-ray diffraction. This may occur because the preparation method has not allowed sufficient time for adsorption and penetration of the galleries to be completed or that dispersive mixing has been insufficient and that if more time is given, the polymer–clay system might develop either fully intercalated or exfoliated structures. The extent of dispersion of clay in polymer depends on intrinsic properties of polymer and clay including aspect ratio of clay platelets, volume fraction of clay, interactions between polymer, clay and clay modifier if present, and processing conditions.[5,16] Generally fully exfoliated polymer–clay nanocomposites are only found in volume fractions of clay lower than 3% due to the small size of clay platelets.[1,5,15]

3. Properties and applications of nanocomposites

The justification for researches in polymer–clay nanocomposites rests on enhancement of polymer properties in five main property areas: mechanical, barrier, flame retardant, electrical, and biodegradable. These have been reviewed widely[17] and are treated concisely here.

Modest additions of clay (4.2 wt%) increased the tensile strength of nylon 6 from 69 MPa to 107 MPa, and the tensile modulus was doubled while retaining impact strength at the level for nylon 6. The heat distortion temperature of the composite was 87 °C higher than that of nylon 6. This significant improvement in mechanical properties of nylon 6–clay nanocomposite was considered to have its origin in the existence of an exceptionally high interfacial surface area and the formation of ionic and/or hydrogen bonds between the organic polymer and inorganic silicate.[1,18] Rao and Pochan have reported the importance of the volume fraction of the constrained polymer phase, which serves as an unmeltable crystalline phase that results in improvement in mechanical properties as well thermal properties.[19] The flexibility and mobility of clay platelets should also be taken into account when interpreting mechanical properties results. For example, when a nanocomposite is under an external stress, the clay platelets contained could bend[15,20] or orient.[6] More detailed discussions on mobility of clay platelets can be found in Section 7.6.

Table 1 shows the mechanical properties of an exfoliated epoxy–clay nanocomposite with only 10 wt% organically-modified magadiite.[5] For an exfoliated epoxy–clay nanocomposite containing 5 wt% clay there was a 25% increase in storage modulus in both glass and rubbery regions.[21] These nanocomposites have been studied for applications as adhesives, coatings, electrical, automotive and aircraft components.[11,22]

Unmodified polyolefin composites are less easy to incorporate in nanocomposites but the Young's modulus of exfoliated clay (5 wt%) with maleated polyethylene was increased by 30% compared to a 9% increase for the corresponding conventional composite.[23] Storage modulus, representing the elastic, stored, strain energy of a viscoelastic material, below the glass transition temperature (T_g) of soft segments in a polyurethane was increased by more than 350% for an addition of 21.5 wt% organically-modified clay.[24] In a silicone elastomer, both the strain at break in tensile mode and toughness of the pristine polymer were increased considerably with clay addition.[25]

The biodegradable polymers such as PCL, polylactic acid (PLA) and thermoplastic starch (TPS) are also reinforced by clay. Young's modulus of PCL was increased from 216 MPa to 390 MPa with 10 wt% of ammonium-treated montmorillonite.[7] Storage modulus of PLA–clay nanocomposite containing 3 wt% organically-treated montmorillonite was increased to more than twice that for the unfilled PLA at all temperatures above and below T_g.[26] Below the T_g, increase in storage modulus is due to clay reinforcement only; while above T_g, the enhancement is due to both reinforcement and extended intercalation at higher temperatures. However, it is often found that storage modulus increases with clay additions more when the test temperature is above T_g than in the lower temperature region.[27] Table 2 summarizes some mechanical properties of these polymer–clay nanocomposites.[6,28–31] A

Table 1 Mechanical properties of an epoxy–clay nanocomposite[a] and pristine polymer[5]

Material	Tensile strength/MPa	Tensile modulus/MPa	Strain at break/%	Yield strength/MPa	Compressive modulus/GPa	Storage modulus at 120 °C/MPa
Polymer	0.5	3.8	23	75.1	1.4	22
Composite	6.0	16.5	48	87.8	1.8	80

[a] Containing 10 wt% organically-modified magadiite.

Table 2 Mechanical properties of biodegradable polymer–clay nanocomposites

Properties	TPS	TPS/NaMMT (5 wt%)	PLA	PLA/Organo-mica (4 wt%)	PCL	PCL/NH_4MMT (4 wt%)
Tensile strength/MPa	2.6	3.3	19	44	17	32
Young's modulus/MPa	4500[a]	8400[a]	208	252	439	540
Elongation at break/%	47	57	845	1150	165	522
Flexural strength/MPa	—	—	86	94	23[b]	30[b]
References	28,29		27,31		6	

[a] Measured using the ultrasonic pulse-echo method. [b] Yield strength.

small amount of clay substantially improves tensile strength, tensile modulus, flexural strength and flexural modulus without loss of elongation at break. For example, with presence of 4 wt% organomica, the elongation at break of PLA increased from 845% to 1150%.

An increase in elongation at break often results in an increased energy at break.[2,32,33] Shah *et al.* found a dramatic increase up to 700% higher than in the neat polymer in toughness and 70% higher in elongation at break of polyvinylidene fluoride nanocomposite with 5 wt% organoclay based on the energy represented by the area under the tensile stress–strain curves.[32] The enhanced toughness was attributed to the structural and morphological changes induced by the clay particles, including the transition of α-spherulites to thin fibre-like β-crystallites which are re-oriented in the strain field.

Similarly, studies on polymer blend–clay nanocomposites show that the presence of clays has resulted in considerable improvement of the mechanical properties. Wang *et al.* show that the peel strength, expressed a force per unit length in a 'T' peel test, of polypropylene/polystyrene (PP/PS) was increased from 523 N m^{-1} to 1768 N m^{-1} and the adhesive fracture energy was increased from 1046 J m^{-2} to 3536 J m^{-2} with 0.5 wt% organically-modified clay.[34] Li *et al.* added 18 wt% organically-modified clay to syndiotactic PS/nylon 6 blends containing 5 wt% sulfonated syndiotactic PS as compatibilizer and found there were considerable improvements in impact, flexural and tensile strengths without loss of elongation at break.[35]

Enhancement of mechanical properties depends on the structure of nanocomposites formed and many papers [*e.g.* [5–7,36]] have reported comparative results based on intercalated and exfoliated structures. At the same or very similar clay loading, an exfoliated nanocomposite often gives a higher elastic modulus and tensile strength because of the high stiffness of clay platelets and good dispersion.[5,6] However a nanocomposite with an exfoliated structure could have a lower toughness than that with an intercalated structure: Dasari *et al.* found a decrease in the Izod impact strength of nylon 6 with the inclusion of 10 wt% nanoclay from 7.1 kJ m^{-2} to 3.2 kJ m^{-2} and 4.3 kJ m^{-2} for the exfoliated and intercalated structures respectively.[37] This was attributed to little or no delamination associated with exfoliated clay platelets, and delamination and the formation of submicron voids associated with intercalated clay tactoids.

Barrier properties are also significantly improved by clay dispersions. The rate of water absorption in nylon nanocomposites was lowered by 40% compared with nylon 6.[5] Polyimides used for microelectronics showed reduced coefficient of thermal expansion by 21% and permeation coefficient of water vapour by 54% with only 2 wt% montmorillonite, retaining the optical clarity of the unfilled polymer.[38] The scattering size of montmorillonite (200 nm) is smaller than the wavelength of visible light (400–700 nm). Nielson's tortuous path model[39] was often used to explain the reduced permeability with presence of clay in polymer.[38,40] Recently this model has been modified by several groups by taking into account the polymer/clay interface[5] and layer aggregation.[41] Nazarenko *et al.* found lower permeability of intercalated PS–clay nanocomposites to oxygen than in intercalated-exfoliated nanocomposites, which was attributed to layer aggregation effects.[41] However, Osman *et al.* claimed that exfoliated clay layers are able to build a barrier for the permeating gas molecules, while the intercalated tactoids do not contribute greatly to the barrier properties.[40] Further work is needed to understand better the mechanisms underpinning the enhancement of barrier properties. As with polyimide–clay nanocomposites, exfoliated epoxy nanocomposites also have a comparable optical clarity to that of the pristine epoxy and their chemical resistance is increased.[5]

Oxygen permeability of the biodegradable polymer PLA was decreased to 35% of its original value in the presence of 4 wt% organically modified mica.[30] The water vapour diffusion coefficient of TPS was decreased to 65% and the temperature at which the composite lost 50% of its mass was increased from 305 °C to 336 °C after the addition of 5 wt% montmorillonite.[28] The zero-concentration diffusion coefficient of water vapour for PCL was also significantly decreased by the presence of montmorillonite.[42] Clay also increases resistance to degradation by light and solvents. The avoidance of structural damage caused by exposure to solvents may represent one of the most important benefits of clay reinforcement in elastomeric polymer technology.[25] The addition of clay to poly(*p*-phenylene vinylene) increased the environmental stability against photodegradation under ambient air conditions, providing this nanocomposite with uses such as light-emitting diodes, photovoltaic and photorefractive devices.[43]

Enhanced flame retardancy is generally found for polymer–clay nanocomposites.[5,44] This is associated with char formation resulting from ceramic clay platelets and the barrier effect of clay platelets to the diffusion of the volatile products formed by thermal degradation. Zheng and Wilkie found that with 10 wt% organoclay, the average heat release rate of polystyrene was decreased by 21% of the value for the pristine polymer.[45] Bourbigot *et al.* found that the heat release rate of nylon 6-made fabric was reduced by 40% with addition of 5 wt% organoclay.[46] However it should be noted that presence

of organic clay modifier could catalyze thermal degradation which somewhat compensates these two effects.[47]

Hydrated gallery cations provide ionic conductivity.[5] The intercalation of polyethylene oxide (PEO) in layered silicates can provide polyelectrolytes that exhibit mixed ionic-electronic conductivity.[48] Thus while conductivity was only detected in Li^+-montmorillonite at temperatures higher than 350 °C, for a Li^+-montmorillonite/PEO nanocomposite, significant conductivity can be measured above 150 °C.[49] Electrical conductivity has been studied in the polyaniline–dodecyl benzenesulfonic acid/clay system.[50] The conductivity increased when the weight ratio of aniline to clay was 1 : 3 because the intercalating polymer adopted a more extended conformation which enhances the free motion of the charge carriers.

Biodegradation of PLA nanocomposites was improved in nanocomposites,[51] a result also found by Ray *et al.* for PLA–clay[30] and poly(butylene succinate)–clay[52] nanocomposites which also showed improved mechanical properties. The combination of improved mechanical and barrier properties, together with controlled biodegradability makes these materials uniquely attractive for biomedical and biodegradable packaging applications. Indeed there is growing interest in using clay to enhance biopolymers such as gelatine,[53] chitosan,[54] poly(*N*-isopropylacrylamide),[55] and poly(D,L-lactide-co-glycolide)[56] for medical applications as well as an explosion of studies on using clays in environmentally-acceptable packaging materials.[52,57]

4. Structure of clays

Clay minerals are an example of a wider class of compounds known as layered materials, which may be defined as ''crystalline material wherein the atoms in the layers are cross-linked by chemical bonds, while the atoms of adjacent layers interact by physical forces''.[58] Both clay sheets and interlayer space have widths in the nanometre range. The predominant naturally occurring cationic clay minerals have alumino-silicate sheets that carry a negative charge, which means that the interlayer guest species must be positively charged (cationic).[59]

4.1 Clay types

Clays are generally classified by structure as allophane, kaolinite, halloysite, smectite, illite, chlorite, vermiculite, attapulgite–palygorskite–sepiolite and mixed layered minerals.[60] Polymer–clay nanocomposites are mainly based on smectite clays because of their swelling properties which result from their capacity to host water and organic molecules between silicate layers, high cation exchange capacities, high aspect ratio and large surface area.[5,61,62] The surface area of a mineral when measured using an adsorption method depends on access to the internal surfaces so that the N_2 BET method generally returns the external area which is typically 15–50 $m^2\ g^{-1}$ for smectite clays.[59,60] The internal surface area is better calculated and is about 620 $m^2\ g^{-1}$.[63,64] Smectite clays consist of units in the form of ''sheets'' or ''platelets'', made up of two silica tetrahedral layers with a central alumina or magnesia octahedral layer. Hydrated exchangeable cations are found in the spaces between lattices, as shown in Fig. 2.[65] The

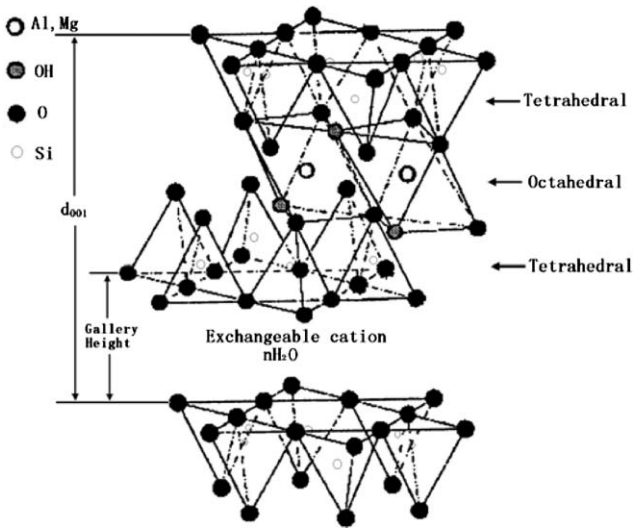

Fig. 2 The structure of 2 : 1 smectite clays; d_{001} refers to basal plane spacing. (Adapted from ref. 65 with kind permission of *Springer Science and Business Media*. Copyright 1992 The Minerals, Metals, and Materials Society).

layers are held together by van der Waals and electrostatic forces and the absence of primary chemical bonds allows the intercalation of water or polar organic molecules, causing the lattice to expand in the c direction.[60]

Montmorillonite and hectorite are commonly used in nanocomposites. They belong to the dioctahedral and trioctahedral groups (two or three aluminium-centred octahedrons in the unit cell respectively) and have ideal chemical formulae of $Al_2Si_4O_{10}(OH)_2{\cdot}yH_2O$ and $Mg_3Si_4O_{10}(OH)_2{\cdot}yH_2O$ respectively.[60] Some Al^{3+} cations in montmorillonite are substituted by Mg^{2+} and similarly some Mg^{2+} cations in hectorite are substituted by Li^+. These substitutions cause charge deficiency and are balanced by external cations present in the galleries such as Na^+ producing chemical formulae $M_{x/n}{}^{n+}{\cdot}yH_2O[Al_{4.0-x}Mg_x(Si_{8.0})O_{20}(OH)_4]$ and $M_{x/n}{}^{n+}{\cdot}yH_2O$-$[Mg_{6.0-x}Li_x(Si_{8.0})\ O_{20}\ (OH,F)_4]$.[62]

If natural montmorillonite is heated to 600 °C or above, interlayer water is lost and there is a reduction in the number of hydroxyl groups in the lattice. The platelets stack together and, at higher temperatures, the structure is disrupted.[60] These changes can be detected by measurement of the basal plane spacing by XRD which collapses to approximately 1 nm[64,66] and by Fourier transform infrared spectroscopy (FT-IR) for loss of the –OH vibrational absorption. Concurrently, step changes in mass and two pronounced endotherms appear in thermogravimetric analysis (TGA) and differential scanning calorimetry (DSC) respectively. The third endotherm typically starts at about 1000 °C[60] and its completion signifies the onset of irreversible crystallographic changes in the clay to form spinel, quartz, cristobalite or mullite. Thus heat treatment can be used to control intercalation in experimental design by producing a clay which has similar chemical constitution but cannot act as a host for intercalated species.

Another potential clay that can act as a control in experiments to compare the properties of hosting and non-hosting particles is kaolinite, which is generally considered as

'non-swelling'.[67,68] It thus provides an experimental resource for comparing the property enhancement provided by nanocomposites to those offered by conventional composites.[69] Kaolinite is a 1 : 1 dioctahedral clay mineral with ideal composition of $Al_2SiO_5(OH)_4 \cdot yH_2O$.[60] The lattice structure of kaolinite is composed of a single silica tetrahedral sheet joined to a single alumina octahedral sheet with the oxygen planes exposed on one side and hydroxyls on the other. Unusually, compared to other clay systems, organic compounds are not so easily intercalated into kaolinite because of the presence of strong hydrogen bonding between the hydroxyls and the oxygens in the two neighbouring layers. Only if it is pre-treated with polar guest species such as dimethyl sulfoxide and *N*,*N*-dimethylformamide can it be intercalated.[70,71]

4.2 Cation exchange

The cation exchange capacity of a clay depends on its crystal size, the pH and the type of exchangeable cation.[62] The exchangeable cation affects the interaction between organic molecules and clay, particularly the likelihood of intercalation or exfoliation, and so provides opportunities to adjust the surface energy and the interaction with organic species by judicious choice of the exchangeable cation.[61,72] Cation-exchanged montmorillonite clays are widely studied[73,74] but the influence on the guest depends on the preparation conditions.[60,61]

4.3 Clay modifiers

Natural montmorillonite is hydrophilic and is generally considered unsuitable for hosting non-polar organic molecules without prior treatment. Interlayer cations can be exchanged with organic cations to obtain organophilic montmorillonite producing an 'organoclay', which has an expanded interlayer spacing and more readily produces a polymer–clay nanocomposite by intercalation and/or exfoliation. Traditional modification agents behave as surfactants such as alkyl and quaternary ammonium halides (*e.g.* dimethyl di(hydrogenated tallow) quaternary ammonium chloride), mainly following the Toyota research group who used a solution of 12-aminolauric acid in concentrated hydrochloric acid as the modifier for montmorillonite to reinforce nylon 6.[1] Similarly, modification is necessary for hectorite to make it organophilic.

The nylon-clay nanocomposites have promoted widespread interest because of their outstanding properties in comparison with the pristine nylon 6. Okamoto *et al.* point out that the reason nylon 6-clay nanocomposites offer substantial property enhancement is that there is a very strong interaction between the matrix and silicate layers through the formation of strong hydrogen bonds.[75] Indeed the Toyota Group claim that increased modulus, sustained strength and impact properties are due to formation of ionic bond between NH_2– and clay sheet.[1] Both hydrogen and ionic bond explanations for the changed properties depend on the amine group that is present in the polymer.

Judicious choice of modifier is central to the development of polymer–clay nanocomposites with high performance. Wilkie *et al.* recently developed new organoclays that were treated with tropylium[76] or triphenylhexadecylstibonium trifluoromethylsulfonate,[77] or that contained oligomeric styrene,[45] methyl methacrylate[78] or ε-caprolactone[79] for reinforcing PS, PE, PP, polymethyl methacrylate and acrylonitrile–butadiene–styrene (ABS). The authors found that these novel organoclays are more stable than the quaternary ammonium treated clays during melt processing with polymers. They are more compatible with the polymers studied and hence better clay dispersion was achieved. Shin *et al.* also introduced bifunctional organic modifiers, alkylaluminium vinyl alcohol to treat clay and found that *in situ* polymerisation of PE with such organoclay led to effective exfoliation of clay platelets and chemical bonding of PE chains to silicate surfaces as assessed by TEM, SEM and DSC.[80] Recently Okamoto and co-workers found that the interlayer expansion of organoclay by intercalation of polymer depends on the initial interlayer opening of the clay, and a small initial interlayer opening leads to a greater interlayer expansion regardless of the polymer matrices, the miscibility between polymer and intercalants, and Lewis-acid strength of the intercalants.[81–83]

It is noted that alkyl or quaternary ammonium-treated clays often decompose at a temperature lower than 200 °C while engineering plastics such as ABS and PET often require processing temperatures close to or higher than 200 °C. Thus development of surfactants with a higher decomposition temperature forms an important part of nanocomposite research as evidenced by many recent studies.[76–80] Zhang *et al.* found that clay modified with styrene, lauryl acrylate and vinylbenzene chloride only has 10% weight loss at 370 °C.[84] Hedley *et al.* found that the clays modified with tetrabutylphosphonium and butyltriphenylphosphonium provide an onset decomposition temperature of approximately 300 °C.[85]

The surfactant used to modify the clay may also have other uses. Thus nanocomposite foams can be produced by reaction between thermoplastic starch (as the matrix) and a quaternary ammonium compound (as the clay modifier) to yield ammonia which acts as a blowing agent.[86] This approach could have wider applications for functional intercalation providing a 'Trojan horse' approach to materials formulation; an idea that parallels the concealment of medicants in the galleries for the purpose of slow or controlled release. Lately Harikrishnan *et al.* found that clays can act as cell openers in polyurethane foam formation.[87] It is widely accepted that carbon nanotubes can also be used as a filler for polymers.[88,89] As a result, there have been attempts to nucleate and grow carbon nanotubes on clay surfaces for this purpose[90] and on incorporating mixtures of nanotubes and clay[91] to enhance polymer properties, with the aim of combining the outstanding properties of both fillers.

5. Preparation methods of nanocomposites

There are three main methods for preparing polymer–clay nanocomposites. They are *in situ* polymerisation,[92,93] solution methods[94] and melt-processing methods.[6,7]

A wide range of polymers is known to form clay nanocomposites: thermoplastic and thermoset, water soluble and organic solvent soluble. The commonly studied polymers include polyglycols,[94] polyethylene oxide,[48,49] polyvinyl chloride,[95] polyolefins,[4,23] polystyrene,[96] polyamides,[1,3] polymethyl methacrylate,[97] polyesters,[98] urethanes,[23] epoxies[99] and polylactic acid.[30]

5.1 In situ polymerisation

For *in situ* polymerisation, clay (in suspension) is directly added to a monomer (in solution), followed by dispersive mixing and heating where appropriate, mostly in the presence of an initiator.[1,42] Okada and Usuki successfully obtained exfoliated nanocomposites of nylon 6 and montmorillonite from the polymerisation of ε-caprolactam in the interlayer space of montmorillonite and dispersion of clay platelets into a nylon 6 matrix.[1] *In situ* polymerisation makes thermosetting polymer–clay nanocomposites possible. For example, poly-[oligo(ethylene glycol) diacrylate] (POEGDA)–clay[93] and epoxy–clay nanocomposites[99] have been prepared using this method.

5.2 Solution methods

In the solution methods, generally the clay (in suspension) is added to a polymer solution, followed by dispersing and heating if appropriate. This method is often used for water-soluble polymers such as PEO, poly(vinyl alcohol) and poly(vinyl pyrolidone) but other solvents such as toluene,[100] chloroform,[101] acetonitrile,[48,49] dimethylacetamide[102] and tetrahydrofuran[76] have also been used. Aranda and Ruiz-Hitzky intercalated PEO into montmorillonite in the presence of different polar solvents and showed that the nature of the solvent is crucial in facilitating the intercalation of polymer into clay galleries, the polarity of the solvent being a determining factor for intercalation.[48,49] Much of the current literature is concerned with the preparation of clay–polymer systems where the volume of clay present in the polymer is fairly low, in the region of 5%, however the present authors have a long-standing interest in materials where the clay fraction is substantially higher, an area of research of particular interest to the oilfield industry.[103,104]

5.3 Melt processing methods

The use of some solvents in a production environment often incurs higher costs and environmentally benign and easily-removed solvents are not always available. Sometimes small solvent molecules rather than the desired macromolecule intercalate into the host clay galleries,[105] a form of molecular gate-crashing! Vaia *et al.* developed simple and direct melt intercalation by pressing the composite at room temperature and annealing at a temperature above T_g to complete the diffusion of macromolecules into the galleries.[96] Direct mixing of polymer melt with clay to allow the migration of macromolecules into clay galleries was also explored.[106] The latter is preferred for bulk processing and makes use of conventional and readily available mixing equipment such as twin-roll mills,[6] extruders[107] and blenders.[95] Thus Zhang *et al.*[107] prepared maleic anhydride-modified polypropylene/organoclay nanocomposites using a conventional twin-screw extruder, and Chen and Evans[29] prepared thermoplastic starch–clay nancomposites using a twin roll mill.

Besides these three methods, others include co-vulcanization,[1,5,108] solid-state intercalation,[109,110] sol–gel,[111] emulsion[112] and supercritical CO_2 fluid[113] methods. Usuki *et al.* found that co-vulcanization of nitrile rubber can produce elastomer–clay nanocomposites with surprising properties.[1,5,108] Usually, the addition of a particulate filler to a polymer increases the viscosity but these authors found that the viscosity of the liquid rubber–montmorillonite system decreased with the clay mineral content and was lower than that of the unfilled system, in sharp contrast to carbon black and other mineral fillers which increase viscosity according to well-known volumetric rules.[114] The rate of the cross-linking reaction was unaffected and was comparable to those rubbers filled with carbon black.[1]

Khaorapapong *et al.* reported solid-state intercalation of two diimines into the interlayer spaces of copper-, nickel- and cobalt-montmorillonites by mixing the diimines and montmorillonites at room temperature. The intercalated molecules of the diimines are thought to form $(ML_2)_n$- type coordination polymers (where M and L represent metal and ligand respectively) in the interlayer spacing of the montmorillonite.[110] Gao *et al.* found that it is possible to expand the interlayer distance of either a hydrophilic untreated layered-silicate or an organophilic clay in a polymer (*i.e.* PEO or PS) simply by blending and compression of the solid mixture.[109]

6. Modelling of nanocomposite structures

There are some situations where the best characterisation equipment available cannot easily access material structures. The occlusion of polymer molecules by clay platelets makes it difficult to access the polymer conformation, adsorption and uniformity of occupancy experimentally. With the disordered and dynamic interlayer present in organoclay systems, computer simulation has become a valuable tool for gaining insight into the structure and behaviour of polymer–clay nanocomposites. Furthermore, since the form of the intercalated/adsorbed polymer is unknown, it becomes very difficult to extract meaningful mechanical properties of the polymer–clay system based on measurements of the phase pure separate clay and polymer systems. As a result, a substantial body of literature is available where computer simulation techniques have been applied to organoclay based material systems; Greenwell *et al.* have recently reviewed the use of computer simulations of clay minerals in a materials chemistry setting,[115] and Boulet *et al.* have recently reviewed the use of electronic structure methods for investigating clay minerals.[116] Here we consider the burgeoning literature, which covers the application of computer simulation techniques, at a variety of length and time scales, to polymer–clay nanocomposite materials. Though these computer simulation techniques can often add valuable information to the description we have of organoclay systems, certain assumptions are generally employed, which may have implications for the conclusions that can be drawn from the results, as shall now be discussed.

In order to understand areas where the underlying assumptions may give rise to misunderstandings during the simulation of polymer–clay systems it is necessary to understand something of the history and development of modelling methods in this area. Many of the approximations and assumptions arise from the scientific approach adopted – it is convenient to reduce the problem to a small size and employ accurate calculations to arrive at structures that conform to chemical

intuition without recourse to considering the structures observed at larger length scales. An example would be that in many molecular dynamics (MD) simulation cells the clay layers are constrained to being rigid. In reality, micrographs of exfoliated and partially exfoliated clay tactoids show the clay sheets to be far from rigid, often adopting fluted or crumpled structures. The failure of rigid clay sheet models to capture the migration of K^+ cations into the tetrahedral layer sites, when there is clear experimental evidence for this, illustrates the problems faced.[117] A further limitation of MD simulations is that the time-scales accessible to simulation are far shorter than that used for many analytical techniques, meaning that unless the system is well equilibrated, comparison with experimental data is difficult.

6.1 Simulation methods and forcefield derivation

The complexity and size of the organic molecules in polymer–clay nanocomposite systems precludes the use of *ab initio* methods, as a rule, other than to understand the interactions between reactive groups, and the interactions between small components and the clay sheets. These electronic methods are, however, very much essential for gaining insight into understanding the role of clays as catalysts.[116,118] As such, the majority of computer simulations of polymer–clay systems are carried out using forcefield based methods, whereby the interactions between the clay, polymer, cations and water molecules are based on a combination of empirical forcefield terms describing bond vibrations, angles, torsions, short- and long-range electrostatic interactions. A problem arises in that very few forcefields exist which can adequately describe the interactions of both inorganic frameworks, especially two-dimensional structures (as opposed to zeolite-type materials) and organic molecules simultaneously. The majority of forcefields have been parameterised to describe either a discrete set of organic molecules, or inorganic frameworks; one such forcefield is the consistent valence forcefield (CVFF).[119] A number of universal forcefields which attempt to describe, at a much more approximate level, the interactions between a wide number of different atom types, for example the Dreiding forcefield.[120] Recently, there have been a number of forcefields explicitly designed to replicate the interactions between clay sheets and associated organic molecules.[121,122] Owing to the lack of detailed structural information about organoclay systems many of the atomistic forcefields employed are parameterised on the basis of information obtained from electronic structure calculations of small fragments of a clay sheet. In initial simulations these fragments were non-periodic clusters of atoms. Improvements arose when the super-cell periodic boundary condition (PBC) approximation was employed.

All of the atomistic molecular dynamics (MD) and Monte Carlo (MC) methods employed today use the super-cell and PBC conditions. The PBC approximation assumes that a small number of atoms, contained in a super-cell (a small number of repeated unit cells) of adequate size to remove symmetry imposed self-interaction effects, sufficient replicated infinitely in all three orthogonal space directions will be an adequate representation of the bulk material. Though it works well for small models, this approach has three main drawbacks; it assumes: (i) that the distribution of interlayer material is homogenous for a given *d*-spacing; (ii) there are no dynamic phenomena larger than the simulation cell; (iii) the effect of edges is minimal and that there is no problem with having the clay sheet constrained by the symmetry of having PBC.

Even with the largest polymer–clay atomistic simulations, of up to several million atoms, it is only just becoming possible to simulate a life-sized clay particle (approximately 50 nm × 50 nm),[123] including the edges in non-periodic clay sheets, and modelling the behaviour of a clay tactoid surrounded by polymer, or actual intercalation, which is a long time-scale process, is still in the future. In order to achieve larger length and time scales, even coarser approximations are made involving approximating several atoms to one ''bead''. The covalently bonded atoms are described by beads linked with simple harmonic functions, whilst non-bonded beads interact through Lennard-Jones type interactions. Such coarse-grained simulations, though not able to capture the atomic structure and interactions, can be used to model systems of real size and time scales, capturing phenomena such as composite failure modes and intercalation.

6.2 Interlayer structure and dynamics in polymer–clay nanocomposites

Generally speaking, organoclay models are built on the basis of data gained from two experimental analytical techniques – XRD and TGA. The XRD gives the averaged spacing between successive clay sheets, while the TGA gives the amount of organic material and water present in the sample. It should be noted that XRD cannot give accurate information on the degree of sample that is exfoliated as mentioned above, or the conformation of the clay sheets, though lack of registry between successive layers is often inferred from the shape of the peaks in the XRD pattern. Small angle X-ray scattering (SAXS) is an analogous method to XRD, however SAXS patterns are collected at very small angles (less than a degree) and are capable of delivering increased structural information on clay–polymer nanocomposites with a resolution of between 1 and 25 nm.[124] Conceptually, SAXS differs from XRD in that the measurements are done very close to the primary beam, *i.e.* at small angles, and as such the technique is usually carried out using X-ray photon beams provided by synchrotron sources. TGA only gives the sample averaged data and cannot readily distinguish between the surface adsorbed and intercalated organic material. The simulation supercell is then set up with the experimentally observed *d*-spacing and the organic content as determined by TGA.

However, it should be noted that coarse-grained mesoscopic simulations show that intercalation of polar organic material may not be homogeneous.[125] The effect of clay edges on polymer intercalation has only been investigated using coarse-grain molecular dynamics, thus far, though ongoing work by the present authors is examining this using large-scale atomistic MD. The results from the simulations show that polymer molecules with head groups that strongly interact with the clay sheets, tend to interact strongly with the clay

sheet edges and, as a consequence do not intercalate readily into the centre of the interlayer. The study found that using a binary polymer mixture, consisting of some strongly interacting, and some weakly interacting, polymer head groups resulted in a more homogenous distribution of intercalated material with the strongly bound material at the clay interlayer periphery, while the weaker interacting material diffused into the inner regions of the interlayer.[125]

6.2.1 Cation dynamics in polymer–clay nanocomposites: lithium ion conduction. Intercalated or non-exfoliated polymer–clay nanocomposites comprise polymer chains sat between clay mineral layers stacked together in a regular arrangement. The study of the dynamics of interlayer cations has been prompted by the postulated use of Li^+–clay polymer systems as a composite polymer electrolyte.[126] Additionally, the dynamics of interlayer cations is accessible through both solid-state nuclear magnetic resonance (NMR) experiment and simulation, thereby providing validation for simulation methods, allowing for the different time regimes.

An initial simulation study of the dynamics of Li^+ in a PEO–montmorillonite system was carried out by Yang and Zax, who used spectral simulation methods to elucidate the line shape of the ^7Li NMR spectra.[127] The study concluded that the main limitation on diffusion in the polymer–clay system was the inefficient coordination of the cations to the PEO backbone oxygen atoms, which resulted in the Li^+ moving along the clay sheets in short jumps, or ''hops''. This study was followed by two studies by Giannelis and co-workers, who performed MC and MD simulations to examine the dynamics of Li^+ and PEO intercalated between layers of the clay mineral montmorillonite, under conditions of varying hydration and layer charge.[128,129] These studies showed that the polymer chains form a bilayer structure, but are relatively disordered in the plane parallel to the interlayer surface. The authors also examined the effect of the presence of a small amount of water in the nanocomposite. It was observed that in the absence of water the cations bind to the interlayer surface, but that when water is present two types of cation environment are discernible, those bound to the interlayer surface, as before, and those hydrated by water in the interlayer region. In both cases, coordination of cations by PEO was minimal. In addition, the calculated diffusion coefficients showed that cations bound to the interlayer surface diffused much more slowly than those hydrated in the interlayer. By examining varying charge (and hence cation content) the authors show that the degree of intercalation of polymer was lower in systems with high cation content as these restricted coordination of the PEO to the clay surface, which is driven by replacement of weakly bound water.

Kuppa and Manias went on to look at the dynamics of Li^+ in both bulk polymer and when confined in the nanometre range galleries of montmorillonite using MD simulation.[130] As in the previous studies, the authors showed that the motion of the lithium cations in the nanocomposites was temperature independent and followed a hopping mechanism, whereby they go from one ditrigonal cavity to another. This is in contrast to what was observed in simulations of lithium cations in bulk PEO, reported in the same paper, which showed a hopping motion at low temperatures and random Brownian-like diffusion at higher temperatures. In contrast to the previous studies, the authors found in their simulations that the Li^+ dynamics was driven by competitive adsorption of the Li^+ between the PEO chains and the clay surface, with correlation between the Li^+ dynamics and the PEO segment dynamics.[130] This study was backed by further experimental studies of ^7Li and ^{23}Na NMR by Reinholdt *et al.*, which confirmed that the dynamics of Li^+ described a hopping type motion, and also suggested that the Li^+ hydration state is unaffected by intercalation of PEO polymers.[131]

Further studies have addressed the interlayer structure, and hence cation arrangements, in polymer–clay systems, however these have not explicitly set out to study the cation dynamics. In the studies reported in this section, the clay sheets have been artificially constrained to rigid structures. As we shall see, this is not necessarily the case, and holding the layer atoms fixed has implications for the transfer of energy in the system.

6.2.2 Structure of interlayer in polymer–organoclay nanocomposites. In many application areas, delaminated or exfoliated nanocomposite are preferred. These comprise of clay mineral layers disordered and dispersed in a continuous polymer matrix. In the synthesis of such polymer–clay nanocomposites it is often necessary to pre-treat the clay mineral by exchange of the natural cations with long-chain alkylammonium ions. This renders the hydrophilic clay mineral layers organophilic, which increases favourable enthalpic interactions with the intercalating polymer and promotes exfoliation. The selection of a suitable alkylammonium ion, that will provide a high interfacial strength between the clay mineral layers and polymer matrix, is however, not always so straightforward. The bulk of simulations of polymer–clay systems address organoclays and the literature in this area may be separated into two groups, (i) those papers addressing the structure of the organoclay only, and (ii) those papers considering the interaction of the organoclay with the polymer.

6.2.2.1 Structure of organoclays. Again using classical MD, Pospísil *et al.* compared the interlayer structure of organo-ammonium surfactants with cetyl pyridinium and cetyltrimethyl ammonium headgroups.[132] These both are of the same length, and form disordered liquid like arrangements; however, the cetyltrimethyl ammonium had far stronger electrostatic interactions with the montmorillonite clay sheets. Zeng *et al.* went on to examine the interlayer structure and dynamics of a range of organo-ammonium surfactants in the interlayer of montmorillonite.[133] The length and number of the hydrocarbon tails were varied. It was found that the ammonium head-group of the surfactants tended to align adjacent to the clay surface, and, depending on the varied parameters, the aliphatic tails formed mono-layers, bi-layers, tri-layers and even pseudo-quadrilayer between the clay sheets.[133] In following work, the structure of the dioctadecyldimethylammonium surfactants in the quadrilayer were further investigated.[134] The difference in diffusion properties of the alkyl chains was monitored; it was found that the diffusion increased towards the tail of the molecules, suggesting more liquid and disordered behaviour. Again, the atomic

coordinates in the clay sheets were fixed during MD in these early studies.

In direct comparison with experimental work, Heinz *et al.* used MD simulations to gain insight into the phase transitions observed in alkylammonium mica, gaining good quantitative agreement.[135] The authors investigated systems at less than 100% cation exchange capacity, and proposed a geometric parameter for the clay surface saturation by the alkyl chains. This study necessitated some forcefield development, particularly with respect to the charges assigned to the system.[136]

In order to determine the suitability of surfactant modified clays for preparing fully exfoliated nanocomposites, Pospísil *et al.* attempted MD simulations to calculate the sublimation energy, interaction energy and the exfoliation energy of simulated octadecylammonium–montmorillonite systems further intercalated with alkyl amine species.[137] Results suggested that the presence of Na^+, and shorter chain length alkyl amines both have a detrimental effect on the exfoliation energy. In a combined experimental/MD simulation study, Paul *et al.* determined that a linear relationship existed between *d*-spacing increase and the mass ratio between organic and clay.[138] Where surfactants had hydroxyl-ethyl units, increased packing density occurred attributed to increase hydrogen bonding between these units and the clay sheets. The authors also identify that the structure of the interlayer in surfactant modified clays is significantly more disordered than many models with parallel alkyl chains, or precisely inclined monomers, might suggest. A forcefield based energy optimisation route was chosen to determine the variation in total energy *versus* the basal spacing for a selection of organo-modified montmorillonite, with the resulting curves being fitted to Morse potentials.[139] Agreement with experimental *d*-spacings was found with three of the surfactants, dimethyl-2-ethylhexyloctadecyl ammonium, bis(2-hydroxyethyl) octadecyl ammonium, benzyl dimethyloctadecyl ammonium salts, but a poor fit was found for the dimethyl dioctadecyl ammonium salt. This study used rigid layers, and did not include thermal effects, so the discrepancy may be due to the lack of molecular motion resulting in the surfactant molecules becoming trapped in local energy minima.[115]

6.2.2.2 Interactions of polymer with organoclays. Tanaka *et al.* performed molecular dynamics and energy minimisation simulations to investigate the interaction of nylon 6,6 with an isolated layer of the clay mineral montmorillonite, treated with alkylammonium ions. These showed that as the molecular volume of the alkylammonium ions increases the binding energy between nylon 6,6 and the clay mineral decreases, while that between nylon 6,6 and the alkylammonium ions increases. In addition, they indicated that the presence of polar functional groups, such as –OH and –COOH, in the alkyl chain of the ammonium ions, increases binding energies with nylon 6,6.[140] Also investigating quaternary ammonium modified montmorillonite nylon 6 composites with atomistic MD simulations, Fermeglia *et al.* showed that the binding energy of the polymer matrix with the clay sheets showed a decrease, as the volume fraction of surfactant was increased. However, the binding between the components, *i.e.* polymer–ammonium salt and ammonium salt–clay increased with increasing ammonium salt content. Again, the presence of polar groups increased the interaction energy between the ammonium salts and the polymer.[141]

Subsequent studies moved away from the nylon 6 systems. Polypropylene organoclay systems have been investigated using MD simulations by Toth *et al.*[142] and Minisini and Tsobnang.[139] In the former work, similar trends as those identified in the study on nylon 6-organoclay, by Fermeglia *et al.*,[141] were found. Minisini and Tsobang examined the interactions between octadecyldimethyl 2-ethylhexyl ammonium montmorillonite and polypropylene using classical MD and showed the presence of maleic anhydride as an additive improved the interactions between polypropylene and the organoclay.[139] The structure and energetics of the biodegradable PCL–organoclay composites have been simulated by Katti and co-workers,[143–145] and by Gardebien *et al.*[146] Gardebien *et al.* systematically varied the amount of PCL and observed that the interlayer adopted a quadriclayer, with a greater portion of extended chain structures relative to a bulk polymer. Examination of the energetics by the authors showed that both polar, and non-polar interactions played a significant role in nanocomposite formation.[146] Similar results were noted for the energetics of caprolactam in 12-aminolauric acid modified montmorillonite by Sikdar *et al.* The organic modifier was found to lie parallel to the clay sheet, and strong non-bonded interactions occurred between the modifier and the polymer. The authors also quantified the relative surface coverage of modifier and intercalated polymer on the clay surface, calculating 54% : 46% respectively.[143] In this study constraints were again placed on the boundaries of the clay sheet, though the boundary perpendicular to the clay sheet was allowed to vary. In a follow-up study, Katti *et al.* used photoacoustic FTIR to gain high-resolution insight into bonding modes within the nylon 6-organoclay nanocomposite, which was then compared with the atomic level detail available from the MD-simulations.[144] Sikdar *et al.* undertook a comprehensive MD simulation examination of the interaction energetics in these systems.[145] It was found that energetically, the polymer organoclay nanocomposite system was more favourable than a mixture of the polymer and clay surfactant and, as previously discussed, non-polar interactions by polymer backbone atoms played a significant role in nanocomposite structure.

Other composite systems have also been investigated, Aleperstein *et al.* used a generic forcefield to energy minimise ethylene–vinyl alcohol copolymer organoclay nanocomposites. The simulations used fixed atomic coordinates in the clay sheets and constrained interlayer separations to examine the interactions between the copolymer and clay surfactant, giving insight to aid interpretation of experimental data, including viscosity measurements.[147]

6.2.3 Simulation of polymer unmodified clay systems. Following on from their earlier work, which addressed the dynamics of Li^+ cations in the clay interlayer, Kuppa *et al.* went on to use MD simulations to examine the structure and dynamics of polymer segments when confined in the clay-interlayer. An initial study compared the behaviour of PEO in Li^+–montmorillonite with that of polystyrene in an

organo-modified octadecyl-ammonium fluorohectorite model; in both cases physisorption of polymer segments to the clay surface resulted in slower segment dynamics.[148] In a further study, the authors examined the effect of the geometric confinement on polymer structure and dynamics, through varying the cation exchange content, and hence number of Li^+ ions in the interlayer. Results showed that increasing cation content had considerable effect owing to the strong interactions between PEO backbone oxygen atoms and the Li^+.[149]

Though long chain alkyl ammonium species can be used to render the clay interlayer more organophilic for intercalating polymers, in instances where low molecular weight primary amines are used, the only interlayer spacing observed corresponds to a monolayer arrangement of organic material. FT-IR analysis of these materials indicated that increased hydrogen bonding was occurring within the interlayer region relative to an analogous primary ammonium intercalated clay, similar to systems where a mixture of ammonium and amine species were co-intercalated.[92]

Simulation studies using large-scale MD methods, with non-rigid clay sheets, showed that at the experimental organic loadings a monolayer of the poly(propylene oxide) diamine monomer forms.[150] If the amine groups are protonated, *i.e.* to form ammonium groups, a conformational change in the monomers occurs, whereby the ammonium cations strongly coordinate with the surface oxygen atoms of the tetrahedral clay sheet and a slight increase in basal spacing occurs in models in which only some of the amine groups are protonated to form the ammonium species, both intra- and inter-molecular H-bonds form between amine N atoms and ammonium H atoms, accounting for the increased H-bonding observed in the FTIR spectra and indicating that a mixture of ammonium and amine species were present in the interlayer of the experimental system, as suggested by the experimental evidence.

During offshore oil well drilling operations, drilling fluids are used to lubricate the drill bit, maintain hydrostatic pressure, suspend cuttings and transfer data readings back to the surface.[103,104] The fluid, which is often water based, contains numerous additives including swelling inhibitors. The latter are used to prevent clay formations, encountered while drilling, from swelling and then either trapping the drill bit or modifying the drilling fluid viscosity through water loss. The swelling inhibitor is often a water soluble oligomer that hinders clay swelling;[150] it is conceivable that, in future, small molecules that polymerise *in situ* may be utilised, creating in the clay what is in effect a high clay fraction clay–polymer composite.[151] Recently, this work has been developed into a new synthetic route for polymer–clay nanocomposites with a high clay fraction by Coveney and co-workers, known as self-catalysed in situ intercalative polymerisation, in which two monomers are intercalated between the clay mineral layers, which then spontaneously copolymerise.[74,92] In a series of combined experimental and theoretical studies, MC, energy minimisation and MD simulations were performed to model the sorption of pairs of organic monomers into the interlayer of the clay mineral montmorillonite. Again, a non-rigid clay model was used. These showed that small organic molecules are easily sorbed into the interlayer. In addition, the observed arrangement of molecules within the interlayer indicated the clay mineral may play the role of an active template that aligns the molecules in a favourable orientation for *in situ* polymerisation. Some evidence for cross-linking between molecular bilayers was also seen. In order to further carry on this work, Boulet *et al.* implemented the clay-organic forcefield, developed by Teppen,[122] within the highly scalable Large Atomistic/Molecularly Massive Parallel Simulator (LAMMPS) MD code, developing parameters for the Li^+ cation.[152]

In order to rationalize reactivity in these systems it is necessary to understand the interlayer arrangement of the reactive centres, where polymerization or cross-linking occurs. Forcefield based simulations have been used to examine issues such as how the nature of the monomer backbone, monomer head-group and identity of interlayer cations affect the arrangement of intercalated monomers.[74,92] For simulated poly(ethylene glycol) (PEG) nanocomposites no evidence was observed for hydrogen-bond interactions between the protons of the PEG alcohol groups and the tetrahedral oxygen atoms of the clay surface.[74] It seems therefore that, in the presence of water and cations, poly(ethylene glycol) is unlikely to form strong H-bonds to the clay surface.

The choice of monomer was also found to affect the cation distribution across the composite interlayer. In the poly(ethylene glycol) composites hydroxyl groups retained some of the cations and associated hydration shells within the mid-plane of the interlayer region. The magnitude of this effect was dependent upon the cation present in the simulated clay composite, with the high surface charge density Li^+ more susceptible than Na^+, while the majority of the K^+ ions migrated to the face of the clay sheet. Snapshots of these systems after 1 ns of MD simulation and the derived 1-dimensional atom density plots, which show the time averaged atom density for the cations relative to the mid plane of the interlayer region, are shown in Fig. 3. Since the cations are retained in the interlayer region they are also more closely associated with the monomer backbone O atoms. Therefore, in the radial distribution functions, the order of interaction for both the poly(ethylene glycol) hydroxyl O atoms and the backbone O atoms with the cations is: $Li^+ > Na^+ > K^+$.[74] Conversely, the authors showed that the poly(ethylene oxide) diacrylate monomers, having no hydroxyl groups, are unable to retain the cations in the interlayer region, resulting in the vast majority of the Li^+ and Na^+ cations migrating into vacancies on the tetrahedral layer of the clay sheet, with the K^+ cations migrating to the face of the clay sheets. This results in the Li^+ cations, effectively charge-shielded by the O atoms at the clay surface and associated water molecules, from interacting with the monomer oxygen atoms. Comparison of the interaction between the different cations and the poly(ethylene oxide) diacrylate backbone and endgroup O atoms confirms this, showing preferential interaction with the low surface charge density cations, *i.e.* in the order: $K^+ > Na^+ > Li^+$.[74]

Poly(ε-caprolactone) intercalated clays are of interest since PCL is a biodegradable polymer, and composites containing it have potential applications in coatings, packaging and tissue engineering as previously mentioned. In a classical MD study, Gaudel-Siri *et al.* examined the interlayer arrangement in Na^+-montmorillonite caprolactone composites. In this

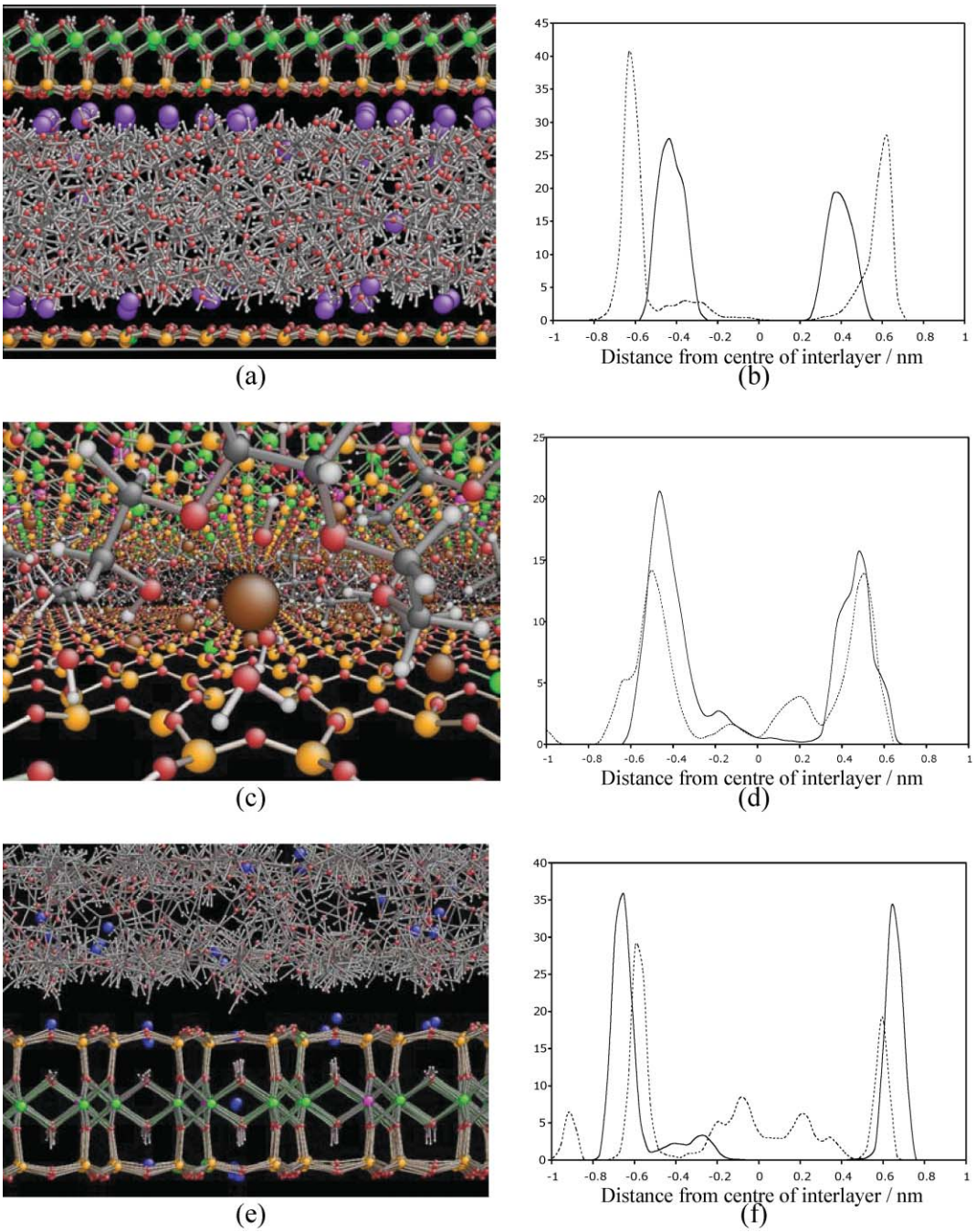

Fig. 3 Snapshots taken after 1 ns of NPT MD simulation showing the interlayer arrangement in poly(ethylene glycol) montmorillonite composites for (a) K^+ is the exchangeable cation; (c) Na^+ is the exchangeable cation; (e) Li^+ is the exchangeable cation; (b, d, f) show the time averaged 1-dimensional atom density plot across the interlayer region for the respective cations, dashed line = poly(ethylene glycol) and solid line = poly(ethylene oxide) diacrylate for comparison. The vertical axes represents relative atom density at any point. Organic material and water content used in the simulations is based on experimental measurements.

study, the clay atoms were constrained. The caprolactone oxygen atoms were observed to replace water in the coordination spheres of Na^+ in the dry clay systems.[153]

There have been studies on clay minerals other than layered silicates. In an unusual study, which looked at organoclay interactions of bulky molecular species, Fois *et al.* examined why the pigments in Maya blue paint are extremely stable. They showed that the indigo dye molecules were incorporated and able to diffuse within the channelled palygorskite clay used within the pigment; however after a period of simulation time the dye molecules reached sites where they became locked into the clay structure and diffusion ceased.[154]

6.3 Electronic structure studies of reactivity in polymer–clay nanocomposites

Interest in the catalytic properties of clay minerals has also arisen out of a desire to better understand and control new

synthetic routes to polymer–clay nanocomposites. Experimental work by Coveney *et al.* indicated that when the natural and unmodified montmorillonite is treated with a solution of methanal and ethylenediamine under mild conditions, the monomers spontaneously copolymerise to form an intercalated polymer–clay nanocomposite material with desirable properties.[104,118] In this context Stackhouse *et al.* performed quantum mechanical density functional theory (DFT) calculations on a periodic montmorillonite model to investigate the catalytic role played by the clay mineral in the reaction.[118] A variety of possible Brønsted and Lewis acid sites were investigated to understand their role in increasing the susceptibility of the methanal C=O carbonyl towards nucleophilic attack. Initial simulations indicated that methanal could only undergo nucleophilic attack by ethylenediamine when suitably activated either by protonation or coordination to a suitable Lewis acid. These studies considered only the interlayer species of the natural clay, various cations and water molecules, and showed that the interlayer cation, when modelled *in vacuo* with the two organic species, could feasibly be sufficiently activating to promote the reaction.[155] Having noted that the interlayer cations and water may have a limited role in clay catalysis, the effect of the structure of the clay sheet was considered. The effect of isomorphous substitution (Al^{3+} by Mg^{2+} or Si^{4+} by Al^{3+}) upon Brønsted acidity of hydroxyl groups located in the octahedral layer, the tetrahedral layer and at edge sites was investigated. Protonation of the methanol molecule was not observed in any of these scenarios, suggesting that the initial step in the *in situ* polymerization reaction was unlikely to be Brønsted acid catalysed. The Lewis acidity of exposed Al atoms at edge sites on the clay sheets was therefore considered. These were shown to exhibit a catalytic effect, the magnitude of which was found to be strongly dependent upon the degree of substitution of Al^{3+} by Mg^{2+} in the octahedral layer of the clay sheets.

There have been other studies where clay–organic interactions have been investigated using electronic structure calculations, but these have not explicitly been aimed at polymer–clay nanocomposites. Aquino and co-workers have looked at the role of cationic clays for the adsorption of organic matter, and also clay catalysed peptide formation.[155,156] The former study was motivated by environmental chemistry considerations, while the latter was driven by prebiotic chemistry. Greenwell *et al.* used DFT and periodic cells to examine the reactivity of *tert*-butoxide intercalated LDHs in *trans*-esterification reactions.[157]

6.4 Accessing material properties and phase-diagrams of polymer–clay nanocomposites using simulation methods

It has been shown that computer simulations can give remarkable insight into the structure of polymer–clay systems. Classical MC and MD simulations can be analysed to give atom density profiles across the interlayer, the distribution of atoms relative to each other and other atoms, power spectra comparable to infra red spectra, diffusion coefficients and visual images of the clay interlayer. All of these data are of much interest to those studying the chemistry and interactions occurring in the polymer–clay nanocomposite system, however in order to design polymer–clay systems with desirable properties *in silico*, it is necessary to be able to calculate the materials properties of the polymer–clay system.

One method by which the elastic properties of polymer–clay systems can be ascertained is by subjecting the cell to stress and measuring the forces. This technique was employed by Manevitch and Rutledge, who used MD to obtain the elastic properties of a single infinite two-dimensional montmorillonite sheets.[158] Katti *et al.* used MD simulations to investigate the mechanical properties of amino acid modified montmorillonite to ascertain their potential for use in polymer–clay nanocomposites. The simulations showed that the system is in the order of three times stiffer when under tension, compared to when placed under compression.[159]

In a recent very large-scale, molecular dynamics study in which montmorillonite composites were modelled with all the atoms allowed to move freely, Greenwell *et al.* reported that visible undulations arise owing to the flexible nature of the clay sheets (Fig. 4).[150] The authors opined that the emergence of these thermal undulations would allow the calculation of materials properties which might be compared with those determined experimentally.[160] Suter *et al.* have followed up this work and utilised distributed high performance multiprocessor machines located within Europe and the USA (exploiting grid computing techniques) to systematically vary supercell sizes up to some 10 million atoms, to investigate these effects in considerable detail within montmorillonite clays.[123] Their results indicate that thermal fluctuations only become apparent in the clay-systems above a certain critical system size, that is finite size effects limit the observation of emergent properties. Direct analysis of the undulations (using methods related to those previously employed for lipid bilayer systems[123]), and coupled stress-strain calculations, allowed the determination of mechanical properties of the clay systems, giving a bending modulus of 1.6×10^{-17} J, which corresponds to an in-plane Young's modulus of *ca* 230 GPa. Using a similar approach, Thyveetil *et al.* also calculated the previously undetermined materials properties of anionic clays (chloride containing layered double hydroxides).[161] The layered hydroxides, having substantially thinner clay sheets, consisting of only mono-octahedral layers, were found to have a bending modulus of *ca.* 1.0×10^{-19} J, which corresponds to an in-plane Young's modulus of 90 GPa for the clay sheets, or 63 GPa for the hydrated system. These developments are important given the current difficulty in determining such materials properties of clay platelets by experimental means.

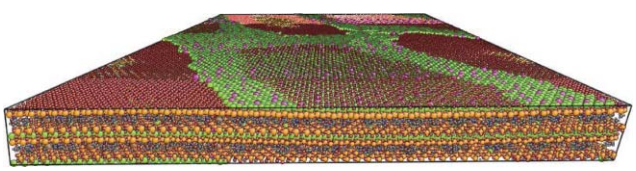

Fig. 4 Snapshot of 350,840 atom supercell (14 × 144 × 2 replication of unit cell) of poly(propylene oxide) diammonium Na^+-montmorillonite after 0.5 ns of MD simulation showing a perspective view of the rectilinear supercell, the clay sheets exhibiting gentle undulations. The colour scheme is: C gray, H white, O red, N blue, Si orange, Al green, Mg magenta, and Na brown. Periodic boundary conditions are imposed in all 3 orthogonal space directions.

Recently, simulation across multiple time and length scales (so called multi-scale modelling) has been employed to study the materials properties of polymer–clay, and other composites. Sheng *et al.* used finite element method based micromechanical calculations to investigate the behaviour and structure of clays at a composite level and also at the level of polymer–clay interactions.[162] Zhu and Narh developed a finite element approach to simulate the tensile modulus of clay based nanocomposites.[163] The authors investigated the effect of the distribution of the clay platelets within the polymer matrix. Results showed that maximum strain occurred in the interlayer near the ends of the clay sheets and increased significantly when the interlayer modulus decreased.

There have been a number of publications reviewing the use of computer modelling at various length and time scales for determining materials properties in nanocomposites in a general sense.[164] In a unique study, Ginzburg and Balazs used a statistical mechanics density functional approach at a coarse particle level to calculate phase diagrams of polymer–platelet systems. The systems studied included both well dispersed isotropic and nematic phases, as well as more ordered intercalated smectic and crystal phases. The phase diagram was determined to be highly dependent on the shape anisotropy of the filler, the polymer chain length and the strength of the interparticle interaction and the qualitative understanding gained is useful for the design and development of novel composites.[165]

6.5 Longer time and length-scales: understanding formation mechanisms of polymer–clay nanocomposites using coarse-grained simulations

As we have seen, simulations with an atomistic level of accuracy can access in the order of a nanosecond timescale and a size range in the order of tens of nanometres, at largest.[123] The molecular dynamics methodology can be extended to include longer times and larger systems by introducing further approximation, *i.e.* coarse graining the parameter set of the forcefields. In coarse grain simulations a number of atoms are counted as one bead – the beads are then connected by simple harmonic functions and inter-molecular interactions are based on Lennard-Jones type functions. Using such methods, Smith *et al.* investigated the matrix-induced interaction between nanoparticles in polymer–clay composites.[166] By assessing the potential of mean force of the system, the authors found that for weaker polymer–nanoparticle interactions, the polymer matrix promoted aggregation, which was overcome when the strength of the polymer–clay interaction was increased resulting in dispersion occurring.

In a comprehensive series of coarse-grained studies, Farmer and co-workers looked at the behaviour of stacks of clay lamellae in both a polymer melt and in a binary fluid (representing a curing agent and a monomer), thereby simulating polymer melt preparation and *in situ* polymerisation preparation methods, respectively.[125,167] Interestingly, the results from the latter intercalation study showed that completely intercalated structures may be formed by simply adjusting the relative concentrations of the binary fluid, or the pressure experienced by the nanocomposite system, with increased swelling suggested by the authors to be indicative of exfoliation observed in some cases.[167] In the simulated polymer melt system, the interaction parameter between the clay sheet and the polymer was adjusted to represent some polymers strongly interacting with the sheet, others having functionalised strongly interacting head groups but weakly attractive (to the clay) polymer segments, and others having no functionality. The studies showed that the strongly interacting polymers "pinned" clay sheets together around the anterior, impeding the fraction of intercalated material. Low intercalation density, and decreased interaction between clay sheets was observed for the end functionalised polymers, as shown in Fig. 5. The highest intercalation density was found for simulations containing a blend of end-functionalised and non-functionalised polymers.[125] As in large-scale molecular dynamics studies, significant distortion of the clay sheets was observed in all these studies.

7. Experimental methods for nanocomposite characterisation

7.1 X-Ray diffraction and electron microscopy

XRD and transmission electron microscopy (TEM) are widely used to assess the degree of swelling of clays and to monitor the formation and structure of nanocomposites. Both have disadvantages. The increase in d_{001} of the clay is taken by most authors as sufficient evidence of successful intercalation by a polymer but it does not measure the amount of uptake (saturation) and there is growing awareness that edge effects or shallow intercalation might displace d_{001}.[125]

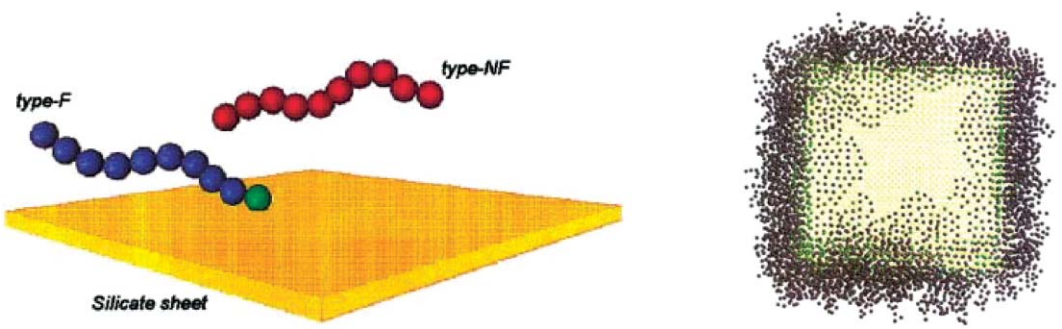

Fig. 5 Coarse-grain MD simulations show polymers with strongly interacting head groups becoming trapped along the edges of clay platelets during intercalation. (Reproduced with permission from ref. 125. Copyright 2003 Wiley Publisher.)

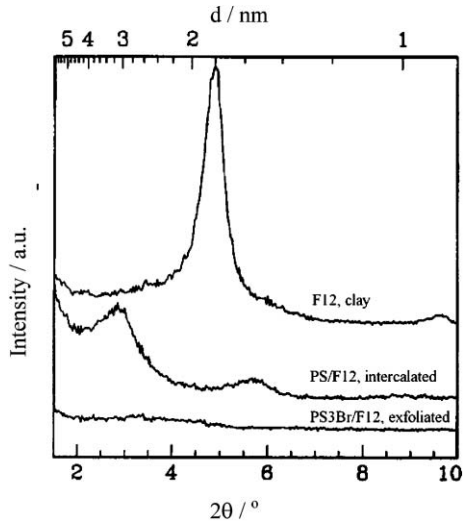

Fig. 6 XRD patterns of polystyrene/fluorohectorite and poly-(3-bromostyrene)/fluorohectorite nanocomposites showing that the (001) reflection shifts to a lower 2θ angle after intercalation and disappears after exfoliation. (Reproduced with permission from ref. 96. Copyright 1996 American Chemical Society.)

The loss of the (001) peak in the XRD trace of the clay can be attributed to the exfoliation of stacked clay layers. It may also be due to low clay volume fraction or even to orientation effects, so a comparison with the other reflections may sometimes be necessary. Individual clay layers can be clearly identified in TEM as having separated but it involves more arduous sample preparation. Ultra-microtome has been widely used for specimen preparation in this area. If TEM samples are too thick, which is often the case when using conventional ultra-microtomes, then the image obtained is very likely to contain overlapping clay platelets or tactoids, making interpretation difficult.

Fig. 6 represents typical, unambiguous examples of what the literature reports as evidence for intercalation/exfoliation. It compares the XRD patterns of polystyrene/dodecylammonium-exchanged fluorohectorite (PS/F12), and poly(3-bromostyrene) (PS3Br)/F12 nanocomposites.[96] The PS/F12 nanocomposite represents an intercalated composite while the latter demonstrates exfoliation. The (001) peaks for PS/F12 and F12 are located at 2θ = 3.0° and 5.5° respectively, corresponding to d_{001} = 2.9 nm and 1.6 nm. The increase in d_{001} indicates an increased gallery height, suggesting the successful intercalation of polymer. In contrast to that of PS/F12, the XRD pattern of PS3Br/F12 was almost featureless, indicating almost full exfoliation has occurred in this nanocomposite.

It is customary to present XRD results as evidence of successful intercalation or exfoliation. Problems can arise in XRD due to the low starting measurement angle, which is often set at 2° of 2θ. For conventional diffractometers using CuKα_1 (λ = 0.15406 nm), this corresponds to d_{001} = 4.4 nm although modern instruments can start at about 1.5° 2θ corresponding to 5.9 nm. The disappearance of the (001) peak of clay can easily be caused by the misalignment of sample holders, wrong slit setting or orientation rather than the exfoliation of the clay layers. So caution should be taken when carrying out these measurements and interpreting the traces. Although XRD is a standard procedure and many operators use CuKα_1 instead of other radiation sources with larger wavelengths such as Co, it is often used at its limits for nanocomposite characterisation. The upper limit on d_{001} should be stated for given instrument settings. According to Jenkins,[168] eqn (1) can be used to select suitable divergence slits:

$$L = \frac{2R \tan(\delta/2)}{\sin \theta} \quad (1)$$

when the divergence angle δ is lower than 4°. L is the illuminated length; θ is the incident angle and R is the goniometer radius.

The problem is illustrated in Fig. 7. In each example, trace 1 is the XRD trace obtained with a well-aligned instrument. A

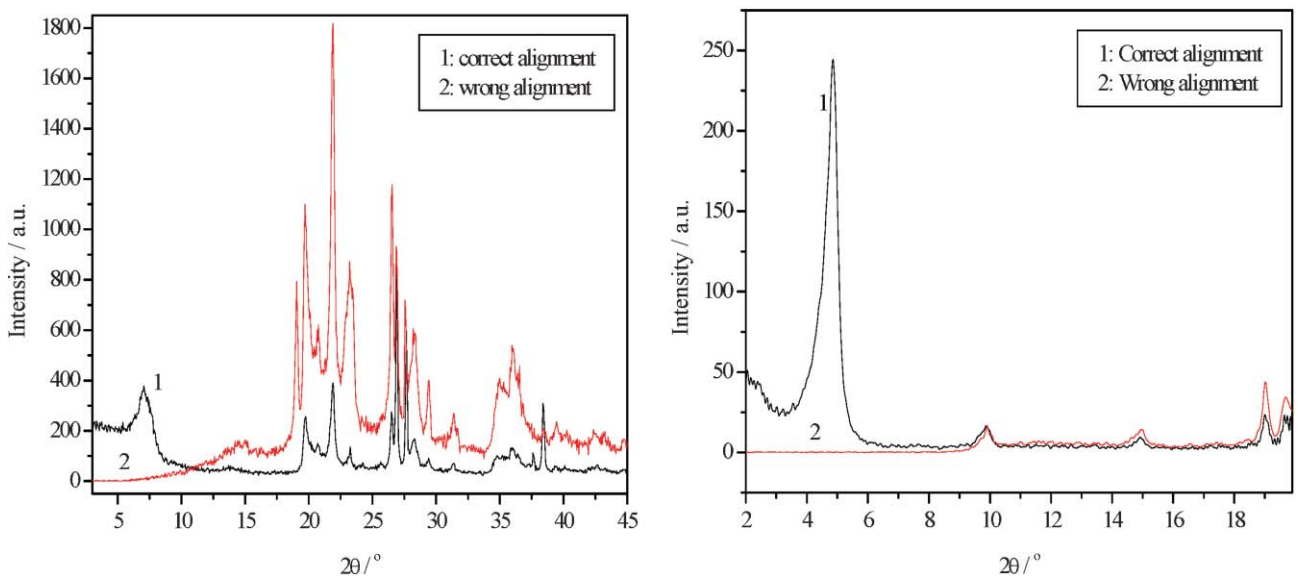

Fig. 7 XRD traces of a) as-received clay with KBr as internal standard; and b) PEG1500–clay nanocomposite showing the effect of placement of sample holders: A slight misalignment of sample holder can lead to disappearance of the (001) peak at these low angles.

slight misalignment is then deliberately introduced (trace 2). The (001) reflection disappears but it would be wrong to infer that the clay had exfoliated. The misalignment does not affect reflections at higher incident angles, which remain but such experiments often collect only the low angles peaks because the interest is in (001). These problems can be avoided with modern SAXS instruments.

TEM is wisely used as a complementary tool to XRD to help determine the nature of nanocomposites. Fig. 8 shows typical images of an intercalated and an exfoliated nanocomposite.[6,169] Under TEM, an intercalated nanocomposite has ordered stacks of layers, which disperse in the polymer matrix as shown in Fig. 8(a). By measuring the minimum distance between layers, corresponding to tactoids perpendicular to the beam, the gallery height can be estimated. For an exfoliated nanocomposite as shown in Fig. 8(b), almost all the clay platelets disperse homogeneously in the continuous polymer phase, presenting as single lines. Also worthy of mention is that shear force was introduced during preparing the sample for Fig. 8(a) while it was absent for Fig. 8(b). The consequence is that one shows orientation and the other is randomly dispersed.

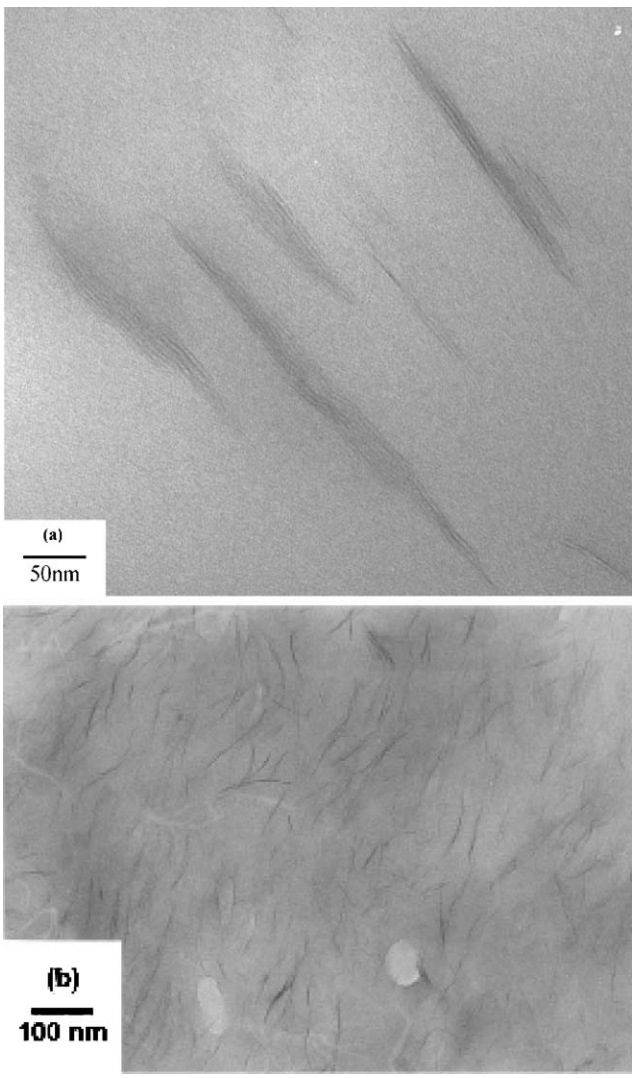

Fig. 8 TEM images of (a) an intercalated nanocomposite in which the clay is present as stacks of several platelets (reproduced from ref. 6. Copyright 2006 American Chemical Society), and (b) a nearly fully exfoliated nanocomposite in which the clay is almost wholly present as single clay platelets (reproduced with permission from ref. 169. Copyright 2001 Elsevier).

Complete intercalation or complete exfoliation is not often seen in nanocomposites. TEM work suggests that most are a mixture of intercalation and exfoliation. An XRD trace which does not employ standards cannot therefore characterise the material and is silent concerning the extent of exfoliation in partially exfoliated systems.

Most "intercalated" polymer–clay nanocomposites contain a low (<0.1) volume fraction of clay filler; they comprise both free bulk polymer and nanocomposite reinforcement. It therefore seems important to characterise them by determining the maximum intercalation amount of polymer in clay as defined by the saturation of the gallery and the maximum loading of clay that polymer can sustain in order to explore the high volume fraction end of the composite range. Also since most nanocomposites include both intercalation and exfoliation, to distinguish these is of great importance for studies on structure–property relationships.

7.2 Measurement of exfoliated fraction

Three principal methods are available to determine exfoliated fraction. Quantitative XRD using a strong and independent reflection from an internal standard can potentially be used to track the decrease in the ratio d_{001} for the clay to the standard peak as exfoliation proceeds. Recently a method based on NMR has been established.[170] Finally, TEM provides an indication but is difficult to use for precise measurement unless very thin specimens are prepared, a large number of images are captured and quantitative microscopy coupled with stereology is used. Recently Vermogen *et al.*[171] developed a statistical TEM image analysis methodology to evaluate the dispersion parameters, which they proposed to couple with optical microscopy for large mapping areas. Rheological testing might also be developed for measurement of degree of exfoliation[172] but at present it can only be used semi-quantitatively.

Since exfoliation does not yield a (001) peak, the change in the peak area after calibration of montmorillonite concentration and sample misalignment should be attributed to exfoliation. Internal standards such as silicon and potassium bromide can be used for calibration. A difficulty is that the initial clay might not be sufficiently well-ordered to give the reference value of peak area for 100% intercalation.

Bourbigot *et al.* developed a method for calculating the dispersion for glassy polystyrene–montmorillonite nanocomposites using solid state NMR based on the proton longitudinal relaxation time (T_1) measurement.[170] It uses two effects: firstly the paramagnetic character of the montmorillonite that directly reduces T_1 of nearby protons, and secondly spin diffusion, whereby the locally enhanced relaxation propagates to more distant protons. The fraction, f, of the actual polymer–clay interfacial area, relative to the maximum possible polymer–clay interfacial area can be determined if a fully exfoliated nanocomposite is also measured. The Al^{3+} cations in the octahedral sheet of montmorillonite are

sometimes substituted by Fe^{3+} which is strongly paramagnetic. The spin–exchange interaction between the unpaired electrons on different Fe atoms produces magnetic fluctuations within about 1.0 nm of the clay surface and the effect on T_1 depends both on the Fe and montmorillonite concentration and on the average distance between the nearest polymer–clay interfaces. Clay layers without polymer interfaces have little influence on T_1 so for more dispersion of platelets, the shorter is the average T_1.[170] When recovering magnetization is plotted against square root of time, the initial slope, when corrected for the contribution from the intrinsic T_1 of the polymer, is proportional to the total polymer–clay interfacial area. Therefore, f can be calculated according to eqn (2).

$$f = \frac{S'}{S'_{\text{exf}}} \times \frac{R_{\text{exf}}}{R} \tag{2}$$

where S' and S'_{exf} are the initial slopes (corrected point by point for the intrinsic relaxation of pure polymer) of a given sample and fully exfoliated sample respectively. R and R_{exf} are the montmorillonite concentrations in the unknown sample and the exfoliated sample respectively.[170] The method is limited to amorphous polymer–clay nanocomposites in which there is no possibility of change in crystallinity which would affect the relaxation time.

7.3 Differential scanning calorimetry: nucleation effects

It is already clear that clay platelets can have several influences on composite properties that extend conventional volume-fraction rules. Where the polymer is semi-crystalline, a fine dispersion of high surface energy platelets can provide heterogeneous nucleation sites. Such nucleating agents, in the form of talc,[173] finely ground phosphate ester salts, carboxylates or adipic acid[174] are routinely added to semi-crystalline polymers to refine spherulite size and increase overall crystallinity. These changes could have a significant effect on elastic modulus that may inadvertently be attributed to mineral reinforcement.

The conventional way to measure crystallinity is to compare the melting enthalpy with that for a notional fully crystalline polymer. The fractional crystallinity is proportional to the measured enthalpy after correction for the mineral mass fraction.[6] The problem is: what change in crystallinity results from the absorption of a significant polymer fraction into the galleries? It is found that the intercalated polymer fraction is often amorphous.[175] Indeed this method has been used to calculate saturation of the galleries.[66,176] Two competing factors influence the DSC result, crystallinity is reduced by intercalation and may be increased by exfoliation. An increase of crystalline fraction from 40% to 45% has been found for PCL organoclay nanocomposites and slightly less for another nanocomposite with a similar clay loading but different organic surfactant.[6] Exfoliated nylon 6-montmorillonite did not exhibit an increase in crystallinity.[1] The contribution to modulus from this source may thus not be as high as expected.

7.4 Analysis of the gallery contents

In an intercalated polymer–clay nanocomposite, the maximum capacity of the clay for intercalation determines the amount of "free" polymer in particle interstices and hence the phase volume distribution. This quantity can easily be found in solution preparation methods by centrifuging, decanting and gravimetric analysis of the supernatant. Even with polymer (*e.g.* PEG) concentrations of 0.01 g ml^{-1}, free PEG was obtained after 5 h treatment time (Fig. 9) suggesting partitioning between gallery surfaces and solution; a phenomenon well known in adsorption studies. The uptake remained approximately constant at 19 wt% when the concentration was higher than 0.023 g ml^{-1}. This trend is consistent with Parffit and Greenland's study[177] which showed that the uptake of PEG by clay follows an L-type isotherm and the timescale of measurement (5 h) corresponds to typical preparation times[178] whereas equilibrium uptake may need longer periods.[177] For example after 168 h, an equilibrium uptake of 33 wt% PEG1500 (molecular weight = 1500) was recorded for PEG concentration of 0.035 g ml^{-1} in water.

The amount intercalated, m_i can also be estimated from DSC measurements for semi-crystalline polymers[66] by judicious use of multiple runs. When a mixture of clay and polymer is run on the DSC twice, the first run allows the polymer to intercalate and the second run only gives the endotherm for melting the excess or "free" polymer since the gallery contents behave as if they are amorphous.[66] This endotherm ΔQ is subtracted from the melting enthalpy ΔH_m corresponding to the initial mass of polymer m_p to provide the amount of amorphous intercalated polymer m_i. The value of m_i is found from ΔQ for the second run (Fig. 10) as follows:

$$m_i = \frac{m_p \cdot \Delta H_m - \Delta Q}{\Delta H_m} \tag{3}$$

Examples of successive DSC traces are shown in Fig. 10 for a mixture of PEG and clay. The first run shows an endotherm (melting) and the overlapping but slightly delayed exotherm (adsorption and intercalation), but the second run only shows a melting endotherm. The third run confirms that the melting

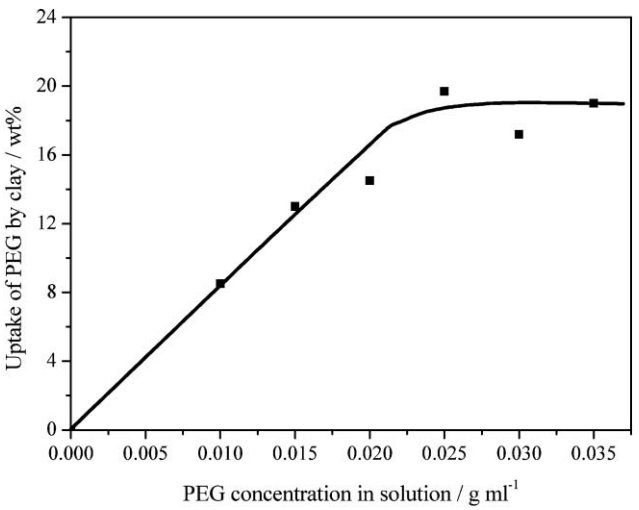

Fig. 9 Curve for the uptake of polyethylene glycol with a molecular weight of 1500 (PEG1500) by clay (t = 18 ks). The line of best fit shows that the uptake of PEG increases with the concentration of PEG in solution and stays constant when the concentration reaches 0.025 g ml^{-1}. (Reproduced from ref. 94. Copyright 2005 Wiley Publisher.)

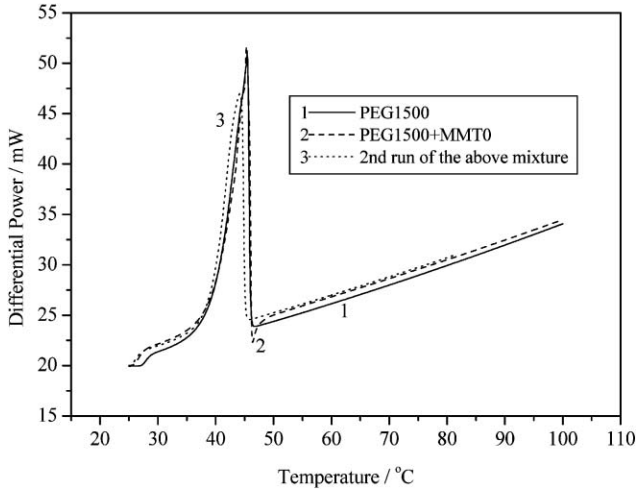

Fig. 10 DSC traces of PEG1500 and a mixture of PEG1500 and clay (MMT0 refers to natural MMT without heat treatment). (Reproduced from ref. 66. Copyright 2005 Taylor & Francis.)

peak area is independent of cooling rate. It should be noted that the intercalation amount is also affected by polymer molecular weight and processing conditions.[94]

Since the polymer–clay interaction involves adsorption, both the intercalation and adsorption of PEG by clay may follow the well-known molecular weight dependence for high molecular weight polymers from solution on high energy surfaces[179] which is expressed as:

$$A = KM^{\alpha} \quad (4)$$

where A is the specific adsorption, M is molecular weight, K is a constant and the index is $0 < \alpha < 0.3$. The results of Parfitt and Greenland[177] for equilibrium uptake of different molecular weight PEG in calcium montmorillonite yield $K = 0.08$ and $\alpha = 0.137$ from which the equilibrium uptakes of PEG with other molecular weights can be inferred.

The exchangeable cation also influences intercalation. For example, the ratio of the uptake of PEG1500 by sodium montmorillonite to that by calcium montmorillonite is about 2.3.[94,177] Therefore the equilibrium total uptakes of PEG with other molecular weights by sodium montmorillonite can be estimated. Nelson and Cosgrove found that the adsorbed amount of PEO by laponite (a synthetic hectorite with a specific surface area of $\sim$900 m^2 g^{-1}) also increases with molecular weight with a power law relationship, $A \sim M^{0.05}$ from small angle neutron scattering studies.[180] They also found that the additional polymer segments accumulate around the edge of the particle rather than on the face; the thickness of polymer layer on the edge being higher than that on the surface. Thus the specific adsorption on the external surfaces (edge and face) should be greater than the intercalation amount on the internal surface (face). This raises interesting questions about the intercalation of high polymers as distinct from water and low molecular mass organic molecules. It is possible that polymers are partially confined at the edges with low gallery saturation and that this is sufficient to cause the swelling detected by XRD. This is supported by simulation work from Sinsawat *et al.* as discussed in Section 6.2.[125] Acosta *et al.* proposed a "frustrated" intercalated structure for the clays modified with large dendritic surfactants, in which the basal plane spacing of clay is not greatly increased and the branched section of the molecules remains outside of the galleries.[181]

7.5 Thermodynamic aspects of intercalation

The general view is that the intercalation of an uncharged polymer in an untreated smectite clay is driven by the entropic increase that results from displacement of adsorbed water as suggested by Theng[61] and reiterated by many other investigators (*e.g.*[101,118]). This is consistent with the experimental observations that water is displaced from the galleries that host the polymer.[48,49,101] Ruiz-Hitzky and Aranda observed that the absorption infrared peaks for hydroxyls and interlayer water in the original clay disappeared on intercalation, indicating loss of these groups and replacement with intercalated PEO, which is supported by TGA results.[48,49] Similarly, Bujdák *et al.* found from TGA and differential thermogravimetry measurements coupled with computer simulations that PEO chains replaced weakly adsorbed water and filled the space between exchangeable cations when using either the melt or the solution methods.[129]

However, experiments on intercalation of dehydrated clays show that without inter-gallery water, PEG can still intercalate into these clays, giving the same d_{001} as that for untreated clay nanocomposites. DSC (Fig. 11) showed that the intercalation of PEG into montmorillonite is exothermic with an enthalpy change of -153 J g^{-1} based on the intercalated polymer and the heat of wetting for the internal surfaces of montmorillonite by PEG is -0.08 J m^{-2} assuming the external surfaces are filled.[66] For the intercalation of PEG into as-received sodium montmorillonite during melting, the enthalpy change (-49 J g^{-1} clay) makes a comparable contribution as entropy change (-45 J g^{-1} clay) to the free energy change. These

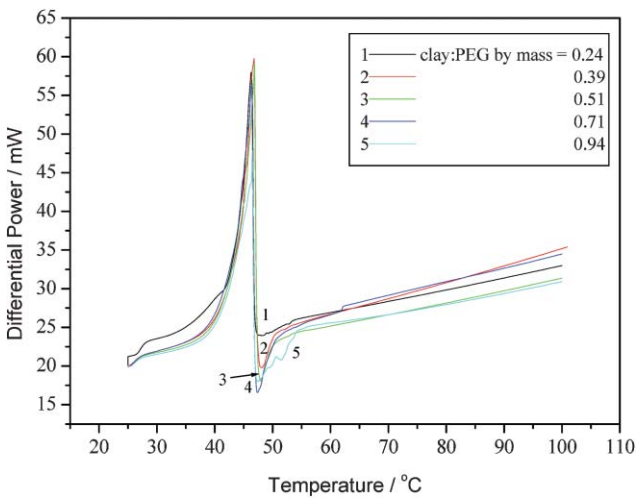

Fig. 11 DSC traces of polyethylene glycol (PEG1500) and clay mixtures during heating: a lid with a hole is placed between the polymer and clay to control the flow of the polymer melt to the clay and hence separate melting endotherm from adsorption exotherm. (Reproduced from ref. 66. Copyright 2005 Taylor & Francis.)

results confirm the observation of re-expansion of heat-treated clays and imply that the reduction in free energy on intercalation results from a significant enthalpic change as well as an entropic change for clays with interlayer water, and primarily from an enthalpic change for clay in the absence of water.

This work is consistent with the hypothesis that the thermodynamic driving force for polystyrene to enter into ammonium-treated clays is the enthalpy change as pointed by Giannelis *et al.*,[96,182] who claimed that a favourable enthalpy change can be achieved by maximizing the magnitude and number of favourable polymer–surface interactions.

7.6 Polymer and platelet mobilities

Without computer simulation methods, much of the discussion of the mobility of adsorbed polymer on high energy, high surface area fillers and of the mobility of the filler themselves in a strain field in a nanocomposite is relegated to the status of speculation. The MD simulation work of Gersappe[183] was stimulated by the observation that in some of the literature, addition of nanoparticles to a polymer results in substantial increases in yield stress and energy to break only if the matrix is above the glass transition temperature, T_g. Improvements in polymers below T_g are modest. The nanoparticle dimensions are comparable to the radius of gyration of the polymer molecule and the timescales for motion of polymer and nanoparticle are similar. Gersappe suggests that the improved mechanical properties result more from the mobility of the particles during deformation than from the stiffening effect of the matrix by the reinforcement as in conventional composites.[183]

Shah *et al.* seem to confirm this modelling by experiments on polyvinylidene fluoride, a piezoelectric polymer, which show pronounced increases in energy absorbed (area under stress–strain curve) when 5 wt% of a clay treated with an ammonium terminated surfactant was added although this is not accompanied by significant increase in yield stress.[32] This improvement only occurred above T_g. Orientation of the tactoids was detected by SAXS and TEM after deformation. In this semicrystalline polymer, the silicate also changes the spherulitic morphology into thin fibre-like crystallites which are also re-oriented in a strain field so there are potentially two toughening mechanisms.

A contrasting idea of a three dimensional network of platelets which forms above a certain percolation threshold is supported by the rheological measurements of Wang *et al.* on maleated polypropylene with up to 5 wt% organoclay.[184] There is an increase in fluidity with clay addition below 2 wt% clay (attributable to the plasticizing effect of the surfactant or to chain scission during processing) followed by a decrease in melt flow index accompanied by an upturn in the molten state storage modulus at low frequencies apparently due to a network of physically jammed tactoids which also restrict molecular motion, in turn retarding crystallisation and thermal degradation and enhancing modulus. In a similar system, Zhong *et al.* show that modulus and restriction on polymer segment mobility both peak at 5 wt% clay but reduce dramatically at higher additions possibly due to loss of exfoliation at higher clay levels as detected by XRD.[185] The role of particle dispersion in controlling mechanical properties in conventional composites is well known; large particles act as crack nucleation sites, very fine particles tend to agglomerate and also behave as critical defects. Thus Thio *et al.*, for example, find that 0.7 μm particles increase toughness by four times while 3.5 μm and 70 nm particles effect no change; all, however, increase Young's modulus which is relatively insensitive to particle dispersion.[186]

There is a general view alluded to above, that the polymer segment mobility is restricted in the region of the matrix adjacent to the reinforcing filler surface. In the case of poly(dimethylsiloxiane)–SiO_2 nanocomposites, dielectric relaxation spectroscopy and DSC show an increase in glass transition temperature and an interfacial layer that is 2.1–2.4 nm in thickness.[187] In a poly(methyl acrylate)–synthetic fluromica nanocomposite, spin–label electron spin resonance shows that the mobility of polymer chains is constrained and the thickness of the rigid interface region is 5–15 nm.[188]

7.7 Effective volume fractions

In a conventional binary polymer–clay composite the volume fraction of the dispersed phase is given by:

$$1/\phi_c = 1 + \rho_c(1 - \mu_c)/\rho_p\mu_c \quad (5)$$

where ρ is density and μ is mass fraction. The subscripts c and p refer to clay and polymer.

However if particle size is sufficiently small, polymer adsorption contributes to the effective volume fraction of the dispersed phase due to a spherical shell of thickness kR_g where R_g is the radius of gyration of the polymer random coil in a good solvent or a melt[189] and k is the fraction of the thickness that behaves effectively as solid. The effective volume fraction of clay, ϕ_c' is then,

$$\phi_c' = \phi_c\,(1 + kR_g\,A_p\,\rho_c) \quad (6)$$

For a clay with specific surface area 38 $m^2\ g^{-1}$ and density 2600 kg m^{-3} a polymer with radius of gyration 10 nm effectively doubles the volume fraction of dispersed phase. Viscosity measurement can sometimes be used to estimate k. If the adsorption energy is high, leading to a "flatter" conformation, then the thickness is less than R_g and if the adsorbate is amphipathic and densely packed leading to a "brush-like" conformation it can be higher.[190]

In such materials, T_g sometimes retains the same value as that for pristine polymer.[191] In other cases, there is a systematic increase in T_g with nano-sized filler loading.[192] A linear increase in T_g with filler loading was seen in the case of rubber–montmorillonite nanocomposites.[193] Similarly in polyvinyl chloride–$CaCO_3$ nanocomposites T_g is shifted towards higher temperatures and thermal decomposition temperatures are increased, further evidence of restriction of segmental and long-range chain mobility due to the large area of high energy filler surface.[194] The elastic modulus of the immobilized polymer may also be influenced. Similarly, diffusion of lower molecular mass organic molecules in the polymer and

permeation of gases are expected to be reduced by the lower mobility of adsorbate as reflected in its higher glass transition temperature. Clearly, since packaging applications are a target for polymer–clay nanocomposites,[6,28] these transport properties are likely to be influenced by adsorption. Bansal *et al.* draw attention to the similarity of constrained polymer between two nanoparticles and thin planar polymer films and suggest that the changes in T_g observed can only be explained by interaction of adjacent interphase layers[195] rather than an adsorbed "third phase" as suggested by eqn (6).

In the case of complete exfoliation, the composite can be treated as a conventional composite for the purpose of finding the phase volume fractions. The main difference from a conventional composite is the adsorption effect. In eqn (6), A_p becomes A_T, the total specific surface area of the platelets and can take values between 658 $m^2\ g^{-1}$ (experimental)[63] and 760 $m^2\ g^{-1}$ (theoretical).[61] Also ρ_c becomes ρ_c^p (the density of clay platelet). The mass and volume fractions of the platelets in bulk clay are 0.94 and 0.80 respectively and the density of bulk clay is 2600 kg m^{-3}.[196] Thus the density of the platelets ρ_c^p is 3067 kg m^{-3}. The platelet density can also be approached in an independent way from experimentally measured gallery area, which is 310 $m^2\ g^{-1}$.[196] This gives $\rho' = 1/(310 \times 10^3 \times h)$ where h is the thickness of platelet. When h = 0.98 nm, ρ' = 3292 kg m^{-3} comparable to that calculated from the density of bulk clay as just discussed. Theoretically, the density of clay platelets can also be calculated from the parameters of the ideal crystal structure and the chemical formula, which gives a density of 2520 kg m^{-3}.[197] However this calculation does not take into account the impurities such as Fe^{3+}, Ca^{2+}, Mg^{2+} and the substituent Na^+ which can account for 11% or more depending on the clay[64] and would increase the true density of clay platelets. Thus eqn (6) becomes:

$$\phi_c' = \phi_c\ (1 + kR_gA_T\rho_c^p) \tag{7}$$

This means the effective solid volume fraction is doubled for the same conditions described above (*i.e.* R_g = 10 nm) if k is only 0.05. This partly explains why a small amount of clay can have strong effect on properties, particularly the transport properties.

In the case of organoclay, the effective volume fraction of exfoliated clay platelets also follows eqn (7) but ϕ_c is then $\mu_c'\mu_c^o/\rho_c^p$ where μ_c' is the mass fraction of the organoclay in the composite and μ_c^o is the mass fraction of clay platelets in the organoclay. To apply eqn (7) in real cases, the value of the coefficient k needs to be found and in exfoliated nanocomposites, where surfactant molecules are adsorbed on the external surfaces of platelets,[105] both competitive adsorption and surfactant–polymer interaction influence the degree of polymer immobilisation.

Comprehensive information is available for the nylon 6 systems as used by Fornes *et al.* which are nearly fully exfoliated and this allows estimates of adsorbed volume fraction to be made.[169] The molecular weight was 29,300 and clay levels were 1.6 wt% to 7.2 wt%. The density of nylon 6 is 1080 kg m^{-3} and R_g is about 7.8 nm based on the bond lengths of C–N of 0.138 nm and C–C of 0.154 nm. Since A_T = 658 $m^2\ g^{-1}$, $R_g{\cdot}A_T{\cdot}\rho_c^p$ is equal to 15.91. This suggests a substantial volume fraction of adsorbate.

A further problem emerges in defining effective volume fraction if the composite is not fully exfoliated. It has been argued that almost all polymer–clay nanocomposites include domains of intercalation among dispersed platelets[15,17] and TEM confirms this[6,15] For an intercalated nanocomposite, the effective volume fraction is influenced mainly by three factors; the absorption of polymer by the clay which increases effective volume fraction of reinforcement, the expansion (reduction in density) of the clay tactoids and the adsorption on the external surface of particles. The last contribution is much lower than the gallery area and is in the region of 15–50 $m^2\ g^{-1}$ depending on the clay as previously mentioned. This effect can be relatively small as in conventional composites.[196]

Intercalated nanocomposites usually consist of intercalated clay tactoids and "free" polymer but it is not clear how "free" this polymer is. The R_g is large enough in comparison with the diameter of tactoids for there to be a tie-chain network which would limit segment mobility between clay tactoids and might even be regarded as a form of physical cross-linking which would be expected to affect mechanical properties. However this effect has not been well understood and it is therefore not considered in the following calculations. In these systems, it is the intercalated clay tactoids that play the role of reinforcement rather than clay particles. The volume fraction of the intercalated phase ϕ_c^i is given by:

$$\frac{1}{\phi_c^i} = 1 + \frac{[1-\mu_c(1+s)](N-1)}{\rho_P\mu_cA[d_2(N-1)+h]} \tag{8}$$

where μ_c is the mass fraction of clay, s is the mass ratio of the intercalating polymer to clay under saturation and A is the specific gallery area of clay. By considering the density of the composite ρ, the volume fraction of intercalated reinforcement is:

$$\phi_c^i = \frac{\rho{\cdot}\mu_c{\cdot}A{\cdot}[d_2(N-1)+h]}{N-1} \tag{9}$$

An alternative approach considers the densities of the nanocomposite and the polymer. The volume fraction of free polymer can then be expressed as:

$$\phi_p^i = \rho[1 - \mu_c(1 + s)]/\rho_p \tag{10}$$

In the case of organoclay, the reinforcement filler is the organoclay intercalated with polymer, namely the intercalated organoclay tactoids. Thus the effective volume fraction of the reinforcement is given by:

$$\frac{1}{\phi_c^i} = 1 + \frac{\rho_c'\left(1-\mu_c'-\mu_c'\mu_c^os\right)\left[d_1'(N-1)+h\right]}{\mu'\rho_p[d_2(N-1)+h]} \tag{11}$$

where ρ_c' refers to the density of the organoclay; and d_1' is the basal plane spacing of the organoclay. The problem here is that the saturation, s, is not readily accessible. Independent experimental methods are needed to estimate this because it is clear from the swelling characteristics of clays that a single value of basal plane spacing from X-ray diffraction may be returned for a wide range of saturation values (*vide supra*).

Examples from the literature indicate the difference between nominal and effective volume fractions. For a predominantly

intercalated nanocomposite[93] using eqn (8) with $N = 8$ and $d_2 = 1.73$ nm (XRD and TEM), $A = 310$ m^2 g^{-1}, $\rho_p = 1220$ kg m^{-3}, $s = 0.18$ and $h = 0.98$ nm, the nominal volume fractions of clay (0.017 to 0.22) correspond to effective volume fractions of 0.026 to 0.32 respectively. Lepoittevin *et al.*[7] studied PCL–organoclay nanocomposites which are mainly intercalated. In eqn (11) using $N = 5$ (TEM), $d_2 = 2.77$ nm and $d_1' = 1.86$ nm (XRD), $\rho_c' = 1870$ kg m^{-3}; $\rho_p = 1140$ kg m^{-3}; $\mu_c^\circ = 0.66$ for the organoclay and taking s as 0.18 g g^{-1} clay, the effective volume fractions are 0.013 to 0.137 for clay platelet contents of 1 wt%, to 10 wt% respectively.

In related work on PCL[6] and assuming the polymer occupies the increased gallery spacing of an organoclay based on the models proposed by Okada *et al.*[1] and LeBaron *et al.*,[25] the effective volume fractions of reinforcement can be found from eqn (11). The parameters are $h = 0.98$ nm, ρ_p and ρ_c' are the densities of PCL and the organoclay which are 1140 and 1700 kg m^{-3} respectively. The mass fraction of inorganic component in the organoclay, μ_c°, is 62.2 wt% for the treated clay according to loss on ignition; μ_c' is the original mass fraction of the organoclay in the mixture and $N = 5$ from TEM. Even though the uptake is unknown, ϕ_c^i turns out to be insensitive to s so that when $s = 0.06$ or 0.2 g g^{-1} clay per layer, the effective volume fractions of reinforcement were unchanged for all but the highest loadings. Making the assumption that s is proportional to the polymer layer number, $s = 0.06$ and 0.2 g g^{-1} per layer are the minimum and maximum bilayer data respectively according to the literature for PEOs,[66,176] *i.e.* 0.11 g g^{-1} for PEO–organoclay nanocomposites and 0.39 (by XRD and DSC) g g^{-1} for PEO–natural clay nanocomposites. Indeed, a deviation of 5 vol% for the highest loading is produced only if s is increased to 0.35 g g^{-1} clay per layer. Taking $s = 0.06$ g g^{-1} per layer for the calculation and an increment in d_{001} of 0.4 nm (monolayer), the calculated effective volume fractions are shown in Fig. 12. This approximation allows volume fractions to be found when s is unknown.

The problem is complicated when the clay is partially intercalated and partially exfoliated. In this case, the composite is composed of intercalated clay tactoids and exfoliated nanocomposites. If the fractional intercalation f_i is known then the volume fraction of the intercalated phase V^i can be found from:[196]

$$V^i = \frac{\mu_c f_i A[d_2(N-1)+h]}{N-1} \quad (12)$$

7.8 Elastic modulus–volume fraction relationships

The elastic moduli of traditional composites are related to volume fraction of reinforcement and to the moduli of the reinforcement and matrix by a range of theoretical and semi-empirical theories.[198–200] To implement these, the modulus of the platelet is needed both for exfoliated nanocomposites and for finding the effective modulus of reinforcing intercalated tactoids.

The elastic moduli of clay platelets have not been measured directly. A review of approaches to this problem indicates that reasonable values can be found by selecting analogous minerals or from numerical modelling.[197] The modelling work[158] gives a relationship between platelet thickness (and hence density) and effective modulus which fits reasonably well to a plot of density *versus* modulus for range of aluminosilicate minerals (Fig. 13). Based on the density dependence, values in the range 178–265 GPa are likely and many investigators have used 178 GPa[6,163] which corresponds to the measured value for muscovite. Provided the clay volume fraction is low (typically < 5 vol%), the value taken for platelet modulus, provided it is in the range 178–265 GPa does not affect the predicted modulus significantly.[197] The Poisson's ratio for montmorillonite can be taken as 0.28 based on literature values for aluminosilicates.[197]

Applying composite volume fraction rules to polymer–clay nanocomposites involves several steps. When the system is predominantly intercalated,[93] the reinforcing "phase" comprises intercalated nanocomposite tactoids. Young's and shear moduli for bulk polymer, gallery saturation (μ_c^i) are needed but the density exerted by the intercalated polymer may be much lower than that of the free polymer.[196] Two approaches are then possible, neither being entirely satisfactory: one is to assume the intercalating polymer still exerts its "free" elastic

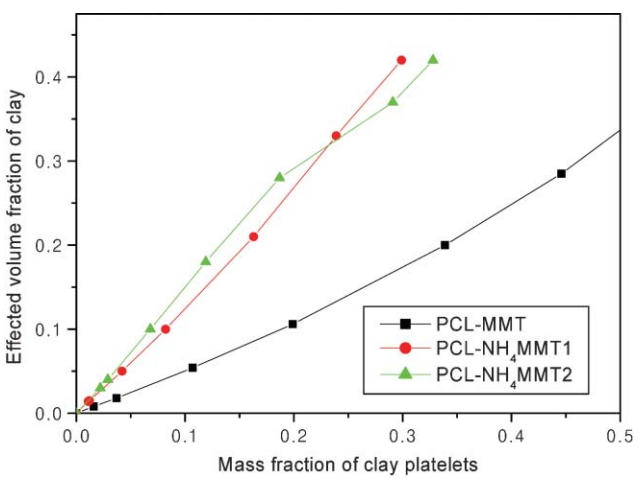

Fig. 12 Effective volume fraction *versus* mass fraction of poly(ε-caprolactone) (PCL)–clay composites.

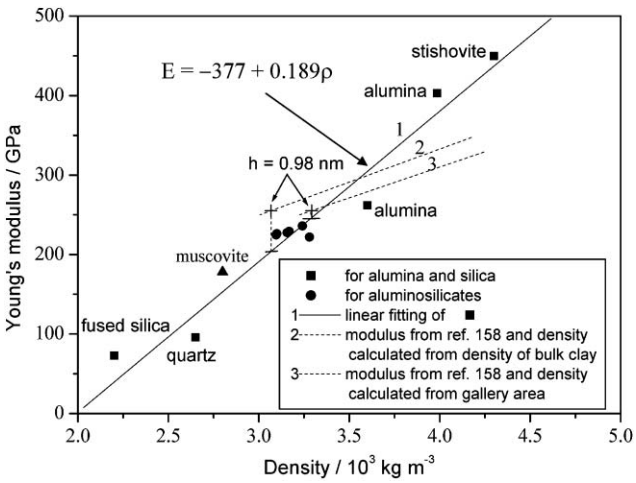

Fig. 13 Young's modulus *versus* density of silica, alumina and aluminosilicates. (Reproduced from ref. 197. Copyright 2006 Elsevier.)

properties. The other is to assume the intercalating polymer exerts its bulk density but leaves a ''porous structure'' in the galleries. Gibson and Ashby's[201] model for a sandwich foam structure can then be applied:

$$E_f = CE_s\left(\frac{\rho_f}{\rho_s}\right)^2 \quad (13)$$

where E_f and E_s refer to the Young's moduli of the foamed core and the solid structure, and ρ_f and ρ_s refer to the densities of the foam and solid. C is a constant including all of the geometric constants of proportionality and it approximates to unity.[201]

Christensen's equations for platelet-filled composites in the two-dimensional case[198] can be used to calculate the elastic modulus of the clay tactoids:

$$G = \frac{1}{t}(t_1G_1 + t_2G_2) \quad (14)$$

$$E = \phi_1E_1 + \phi_2E_2 + \frac{\phi_1\phi_2E_1E_2(\upsilon_1 - \upsilon_2)^2}{\phi_1E_1(1-\phi_2 2) + \phi_2E_2(1-\upsilon_1^2)} \quad (15)$$

where G is shear modulus, t is thickness of the alternating material, υ is Poisson's ratio and ϕ is volume fraction. Subscripts 1 and 2 refer to the clay and polymer respectively. This approach is quite forgiving because when platelet moduli in the range 178 GPa–265 GPa are inserted, eqn (13) and (15) give values of modulus for the intercalated tactoid which differ by no more than 1 GPa for the two approaches.[196] Thus the elastic modulus for the intercalating polymer at reduced saturation in the galleries may not affect the modulus of the nanocomposite very much because of the large difference between the moduli of clay platelets and polymer. In other respects, the inaccessibility of this problem invites a molecular modelling approach.[123]

The final stage is to apply the calculated properties of the intercalated reinforcement in the Hashin–Shtrikman (H-S) bounds.[200] For a two-phase material, the H-S lower and upper bounds for the effective bulk modulus (K_L and K_U) and shear modulus (G_L and G_U) are given by:[200]

$$K_U = K_1 + \frac{(K_2 - K_1)\cdot(1-\phi_1)}{1 + (K_2 - K_1)\cdot\phi_1/\left(K_1 + \frac{4}{3}G_1\right)} \quad (16)$$

$$K_L = K_2 + \frac{(K_1 - K_2)\cdot\phi_1}{1 + (K_1 - K_2)\cdot(1-\phi_1)/\left(K_2 + \frac{4}{3}G_2\right)} \quad (17)$$

$$G_U = G_1 + \frac{(G_2 - G_1)\cdot(1-\phi_1)}{1 + 2(K_1 + 2G_1)\cdot(G_2 - G_1)\cdot\phi_1/5G_1\left(K_1 + \frac{4}{3}G_1\right)} \quad (18)$$

$$G_L = G_2 + \frac{(G_1 - G_2)\cdot\phi_1}{1 + 2(K_2 + 2G_2)\cdot(G_1 - G_2)\cdot(1-\phi_1)/5G_2\left(K_2 + \frac{4}{3}G_2\right)} \quad (19)$$

Fig. 14 shows that the experimental data are very close to the lower bounds when the platelet modulus is in the range 178 GPa–265 GPa. Indeed, it is usual for the elastic modulus of reinforced composites to be close to the lower H-S bound [*e.g.* ref. 202]. The variation in platelet modulus does not seem to affect the predicted results due to the large difference in the modulus of the filler and matrix. Hence Fig. 14 implies that the elastic modulus of nanocomposites can be interpreted using well-established theory provided that the effective reinforcement volume fraction is found.

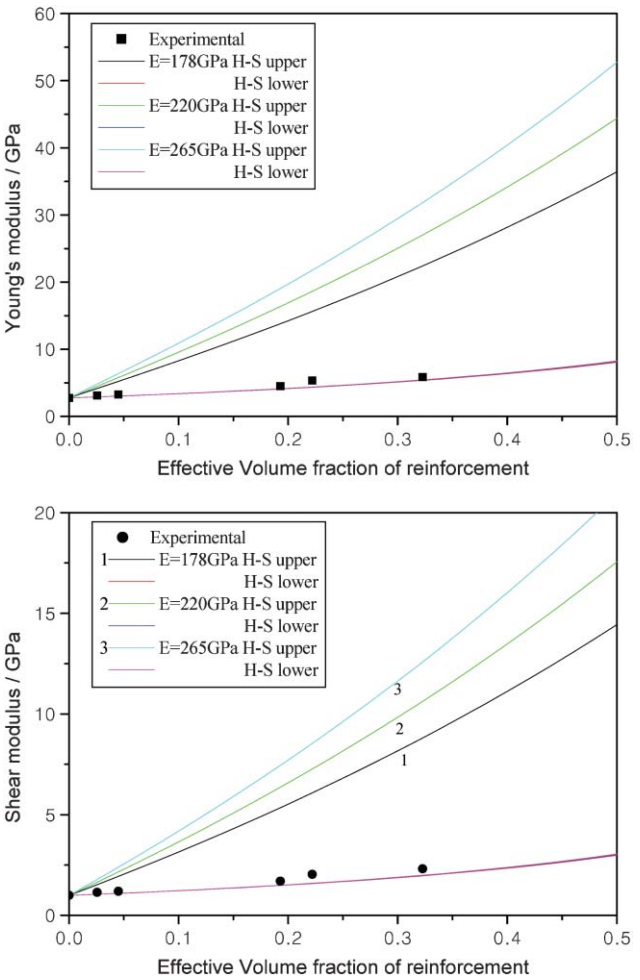

Fig. 14 Elastic modulus *versus* effective volume fraction of reinforcement for poly[oligo(ethylene glycol) diacrylate]–clay nanocomposites showing the experimental data tend to follow the Hashin–Shtrikman lower bound for composite materials.

Following a similar procedure for a PCL biodegradable nanocomposite with a surfactant treated clay and treating the modulus of the surfactant as that for PCL, Christensen's equations for two-dimensional platelet-filled systems as given by eqn (14) and (15), provide the elastic modulus of the reinforcing tactoids in PCL–clay nanocomposites, assuming full saturation. When using this value in the lower H-S bound (*cf.* eqn 17 and 19) the experimental data are very close to the lower bound as shown in Fig. 15 as is often true for binary-phase composites with fillers having much higher moduli[202] and therefore follow the same volume-fraction dependence of properties as other particle-filled composites.

The data for conventional PCL–MMT nanocomposites can be used as a comparison. Since polymer does not enter the clay

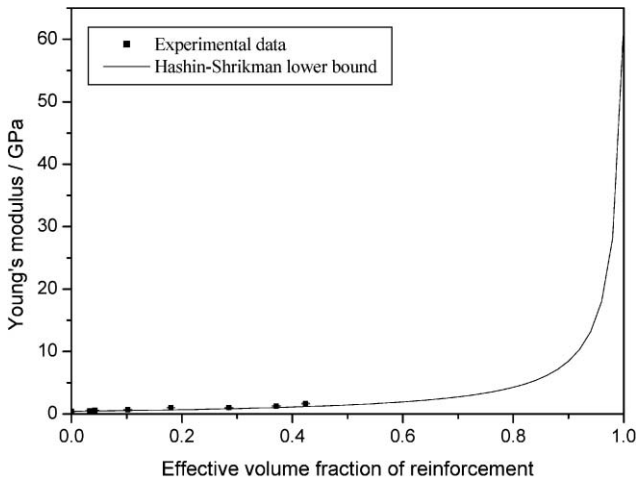

Fig. 15 Young's modulus *versus* effective volume fraction of reinforcement for PCL–NH_4MMT nanocomposites.

galleries, the equi-axed bulk clay particles act as the reinforcement filler. Shear and bulk moduli of the conventional composites were calculated using Benveniste's model[203] which is identical to Christensen's model[204] for bulk modulus K:

$$K = K_2 + \frac{(K_1 - K_2)\cdot\phi_1}{1 + (K_1 - K_2)\cdot(1-\phi_1)\Big/\left(K_2 + \frac{4}{3}G_2\right)} \quad (20)$$

$$G = G_2 + \frac{(G_1 - G_2)\cdot\phi_1}{1 + (G_1 - G_2)\cdot(1-\phi_1)\Big/\left[G_2 + \frac{G_2(9K_2 + 8G_2)}{6(K_2 + 2G_2)}\right]} \quad (21)$$

These two equations are the lower Hashin–Shtrikman bounds,[200] as already noted by Christensen.[204] Young's moduli were calculated using the relation $E = 9KG/(3K + G)$ and plotted as a function of volume fraction in Fig. 16 where they fall between the Hashin–Shtrikman bounds.[200] The H-S–Lielens method[205] applies a coefficient, which is a function of

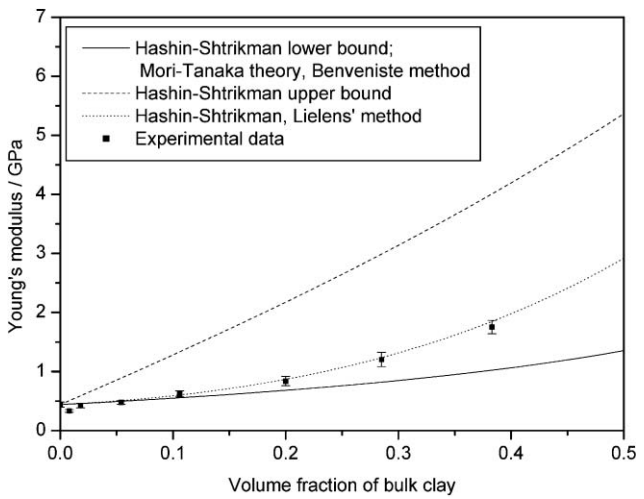

Fig. 16 Young's modulus *versus* volume fraction of clay for PCL–MMT conventional composites. (Reproduced from ref. 6. Copyright 2006 American Chemical Society.)

the volume fraction of the reinforcement filler, $(\phi_1 + \phi_1^2)/2$, to the upper and lower Hashin–Shtrikman bounds: the values of the moduli for composites determined in this way agree with the experimental data very well. This method has been deemed successful by others.[206] The fact that nanocomposites fit the behaviour of other "conventional" composite materials with large-scale reinforcement means that the established equations for composite properties can be used for prediction of nanocomposite properties.

8. Summary and conclusions

Polymer–clay nanocomposites provide a new and important category of polymeric composites. With excellent mechanical and transport properties, they not only have the potential to enhance the performance of pristine polymeric materials but could also replace some of the existing metallic or other composite materials. A small addition of an appropriately pretreated clay, typically less than 5 vol%, substantially enhances mechanical and barrier properties of polymers with little loss of optical clarity. Ionic and electrical conductivity of conducting polymers and biodegradability of polymers can also be improved by the addition of clay. Moreover, the presence of small amounts of clay produces nanocomposites which can be processed in the same way as the unfilled polymer.

Natural smectite clays are hydrophilic and are traditionally treated with quaternary ammonium salts to render them organophilic. In this way, they are compatible with most hydrophobic polymers and make intercalated and exfoliated nanocomposites. There is an ongoing quest for thermally stable surfactants which will sustain melt processing at the temperatures used for processing thermoplastics. Polymer–clay nanocomposites are prepared mainly by *in situ* polymerisation, melt processing and solution methods. Their structure and morphology is generally characterised by XRD and TEM and there is growing awareness that TEM studies are needed to augment XRD because the latter does not disclose the extent of exfoliation.

Clay often acts as a nucleating agent for crystallization of semi-crystalline polymers. However the intercalating polymers tend to become amorphous and, if their elastic modulus thereby decreases, this would compensate for the increase in crystallinity, and hence modulus of the bulk polymers remaining outside of clay galleries. The amount of polymer absorbed within clay galleries increases with polymer molecular weight. It is also affected by the type of exchangeable cations in clay galleries. Thermodynamic driving forces for intercalation of polymer into clay involves both entropic and enthalpic contributions as determined using DSC, FTIR, TGA and molecular simulations.

Taking into account the immobilization of macromolecules on large clay surfaces, the effective volume fractions of clay filler are much greater than the nominal volume fractions which are directly calculated from masses and densities of polymers and clays. This accounts for changes in viscosity and in the diffusion and permeation of gases and liquids in the nanocomposite. If the redefined volume fraction and corrected modulus of intercalated clay filler are used, elastic modulus–volume fraction relationships in nanocomposites can actually

be understood using theories for traditional composites. This may imply that other properties could also be interpreted using abundantly available and well-established theories for traditional composites thus assisting in the understanding of these new and promising materials. However changes in polymer and clay mobilities as well as polymer structure still need consideration when using these theories.

The main directions for current research include: i) preparation of organoclays that are stable at high processing temperatures especially for engineering plastics; ii) synthesis of appropriate surfactants and discovery of well-dispersed polymer–clay nanocomposites, preferably by full exfoliation in most cases; iii) gaining a full understanding of nanocomposite formation, thus allowing the tailoring of structure; iv) the ability to assess quantitatively and quickly the degree of intercalation and exfoliation in nanocomposites providing more comprehensive information on the structure and hence enabling studies of structure–property relationships; v) to improve or retain toughness of polymers after addition of clay; an increasingly important issue since impact strength, in particular, is a primary selection criterion for engineering applications of industrial polymers and presently addition of clay does not always promote toughness whilst enhancing stiffness.

Biodegradable polymer–clay nanocomposites have recently attracted great interest since they are environmentally acceptable; some of the biodegradable polymers are deemed too compliant and therefore benefit from clay reinforcement. This area is expected to expand further in biodegradable packaging and medical applications such as drug delivery and scaffolds for tissue engineering. Such biodegradable composites could also be developed to replace existing engineering plastic materials, for example by conferring enhanced toughness and stiffness *via* addition of clay as well as where appropriate, drawing on biodegradable polymer copolymers and blends.

Computer simulation has provided insight into the interlayer structure, dynamics and reactivity of polymer–clay systems, each of the simulation techniques has an inherent set of approximations and underlying assumptions. Often these approximations and assumptions are not clearly defined for the non-specialist and this article has sought to fill this lack. A move away from MD simulations where the atoms in the clay sheet are fixed has resulted in further insight gained from simulation through the dynamical motion of the clay sheets and, recently, the calculation of mechanical properties.

Current advances in the computer simulation of polymer–clay nanocomposite systems are arising through the increasing amount of computational power available to researchers. These increases do not just arise through faster processors, but also the development of high-end multi-processor computing systems with fast inter-processor communication. These high-end facilities are now being further expanded through grid computing infrastructure, for which novel software now exists to facilitate user uptake[207] Such approaches allow the length and time-scales of any level of description to be significantly extended. Simultaneous with advances in computing technology come advances in theory, allowing different levels of simulation to be ''coupled'' together not just in a hierarchical fashion, where only the end output from one level is fed to the next,[208] but also dynamically,[209] whereby more accurate simulations are ''called'' as required. As simulation size increases, analysis becomes more difficult and visualisation of the simulation becomes ever more desirable, albeit challenging. One of the challenges facing scientists will be to develop methods to analyse the large-scale simulations fully; interactive ''steered'' simulations and immersive visualisation are likely to be employed.[210]

In conclusion, the last 20 years has seen an explosion of interest in lightweight materials based around nanocomposite technology. Owing to the increase in desirable materials performance for smaller filler volumes, and corresponding lower weights, these nanocomposite materials have found uses in weight critical applications such as those in the automotive and space industries. Understanding of polymer–clay (and other) nanocomposite materials at both the molecular level and the composites theory levels not only allows the prediction of materials properties in a given system, but also permits the non-destructive prediction of modes of failure – a very important consideration given the uses these materials are currently put to.

Acknowledgements

The authors are grateful to the Engineering and Physical Sciences Research Council for support under Research Grant numbers GR/R30907 and GR/T24166. The work described in this review was also partially supported by EPSRC (GR/T27488/01); National Science Foundation under NRAC Grant MCA04N014, and the DEISA Consortium (co-funded by the EU, FP6 Project 508830) within the DEISA Extreme Computing Initiative (www.deisa.org).

References

1 A. Usuki, Y. Kojima, M. Kawasumi, A. Okada, Y. Fukushima, T. Kurauchi and O. Kamigaito, *J. Mater. Res.*, 1993, **8**(1179), 1185; A. Okada and A. Usuki, *Mater. Sci. Eng., C*, 1995, **3**, 109; A. Okada and A. Usuki, *Macromol. Mater. Eng.*, 2006, **291**, 1449.
2 U. Gurmendi, J. I. Eguiazabal and J. Nazabal, *Compos. Sci. Technol.*, 2006, **66**, 1221.
3 Y.-C. Ahn and D. R. Paul, *Polymer*, 2006, **47**, 2830.
4 S. K. Swain and A. I. Isayev, *Polymer*, 2007, **48**, 281.
5 *Polymer-clay nanocomposites*, ed. T. J. Pinnavaia and G. W. Beall, John Wiley & Sons Ltd, Chichester, 2000.
6 B. Chen and J. R. G. Evans, *Macromolecules*, 2006, **39**, 747.
7 B. Lepoittevin, M. Devalckenaere, N. Pantoustier, M. Alexandre, D. Kubies, C. Calberg, R. Jerome and P. Dubois, *Polymer*, 2002, **43**, 4017.
8 T. G. Gopakumar, J. A. Lee, M. Kontopoulou and J. S. Parent, *Polymer*, 2002, **43**, 5483.
9 D. Hull, *An introduction to composite materials*. Cambridge University Press, Cambridge. 1981, p. 3.
10 W. J. Work, K. Horie, M. Hess and R. F. T. Stepto, *Pure Appl. Chem.*, 1985, **76**, 1985.
11 T. B. Tolle and D. P. Anderson, *Compos. Sci. Technol.*, 2002, **62**, 1033.
12 S. S. Ray, K. Okamoto and M. Okamoto, *Macromolecules*, 2003, **36**, 2355.
13 H. G. Jeon, H.-T. Jung, S. W. Lee and S. D. Hudson, *Polym. Bull.*, 1998, **41**, 107.
14 K. Wang, S. Liang, J. Deng, H. Yang, Q. Zhang, Q. Fu, X. Dong, D. Wang and C. C. Han, *Polymer*, 2006, **47**, 7131.
15 A. B. Morgan and J. W. Gilman, *J. Appl. Polym. Sci.*, 2003, **87**, 1329.

16 S. Ingram, I. Rhoney, J. J. Liggat, N. E. Hudson and R. A. Pethrick, *J. Appl. Polym. Sci.*, 2007, **106**, 5; A. Boukerrou, J. Duchet, S. Fellahi and H. Sautereau, *J. Appl. Polym. Sci.*, 2006, **102**, 1380; P. H. Nam, M. Kaneko, N. Ninomiya, A. Fujimori and T. Masuko, *Polym. Int.*, 2006, **55**, 916; S. Tanoue, L. A. Utracki, A. Garcia-Rejon, P. Sammut, M. T. Ton-That, I. Pesneau, M. R. Kamal and J. Lyngaae-Jorgensen, *Polym. Eng. Sci.*, 2004, **44**, 1061.
17 M. Alexandre and P. Dubois, *Mater. Sci. Eng., R*, 2000, **28**, 1; S. S. Ray and M. Okamodo, *Macromol. Rapid Commun.*, 2003, **24**, 815; B. Chen, *Brit. Ceram. Trans.*, 2004, **103**, 241.
18 P. Maiti and M. Okamoto, *Macromol. Mater. Eng.*, 2003, **288**, 440.
19 Y. Rao and J. M. Pochan, *Macromolecules*, 2007, **40**, 290.
20 L. F. Drummy, H. Koerner, K. Farmer, A. Tan, B. L. Farmer and R. A. Vaia, *J. Phys. Chem. B*, 2004, **107**, 17868.
21 C. S. Triantafillidis, P. C. LeBaron and T. J. Pinnavaia, *J. Solid State Chem.*, 2002, **167**, 354.
22 J.-S. Chen, M. D. Poliks, C. K. Ober, Y. Zhang, U. Wiesner and E. P. Giannelis, *Polymer*, 2002, **43**, 4895.
23 T. G. Gopakumar, J. A. Lee, M. Kontopoulou and J. S. Parent, *Polymer*, 2002, **43**, 5483.
24 K. J. Yao, M. Song, D. J. Hourston and D. Z. Luo, *Polymer*, 2002, **43**, 1017.
25 P. C. LeBaron and T. J. Pinnavaia, *Chem. Mater.*, 2001, **13**, 3760.
26 S. S. Ray, K. Yamada, M. Okamoto, Y. Fujimoto, A. Ogami and K. Ueda, *Macromolecules*, 2002, **35**, 3104.
27 L. Z. Liu, K. Q. Chen and D. Y. Yan, *Eur. Polym. J.*, 2003, **39**, 2359; N. N. Bihiwankar and R. A. Weiss, *Polymer*, 2006, **47**, 6684.
28 H.-W. Park, W.-K. Lee, C.-Y. Park, W.-J. Cho and C.-S. Ha, *J. Mater. Sci.*, 2003, **38**, 909–915.
29 B. Chen and J. R. G. Evans, *Carbohydr. Polym.*, 2005, **61**, 455.
30 S. S. Ray, K. Yamada, M. Okamoto, Y. Fujimoto, A. Ogami and K. Ueda, *Chem. Mater.*, 2003, **15**, 1456.
31 J. H. Chang, Y. An, D. H. Cho and E. P. Giannelis, *Polymer*, 2003, **44**, 3715.
32 D. Shah, P. Maiti, E. Gunn, C. A. Batt, D. J. Jiang and E. P. Giannelis, *Adv. Mater.*, 2004, **16**, 1173.
33 G. Basara, U. Yilmazer and G. Bayram, *J. Appl. Polym. Sci.*, 2005, **98**, 1081.
34 Y. Wang, Q. Zhang and Q. Fu, *Macromol. Rapid Commun.*, 2003, **24**, 231.
35 H. M. Li, Z. G. Shen, J. Wang, F. G. Zhu and S. Lin, *Acta Polym. Sinica*, 2003, **26**, 78.
36 W. J. Boo, L. Sun, J. Liu, E. Moghbelli, A. Clearfield, H. J. Sue, H. Pham and N. Verghese, *J. Polym. Sci., Part B: Polym. Lett.*, 2007, **45**, 1459.
37 A. Dasari, Z. Z. Yu and Y. W. Mai, *Macromolecules*, 2007, **40**, 123.
38 K. Yano, A. Usuki, A. Okada, T. Kurauchi and O. Kamigaito, *J. Polym. Sci., Part A: Gen. Pap.*, 1993, **31**, 2493.
39 L. Nielsen, *J. Macromol. Sci. (Chem.)*, 1967, **A1**, 929.
40 M. A. Osman, V. Mittal, M. Morbidelli and U. W. Suter, *Macromolecules*, 2006, **37**, 7250.
41 S. Nazarenko, P. Meneghetti, P. Julmon, B. G. Olson and S. Qutubuddin, *J. Polym. Sci., Part B: Polym. Lett.*, 2007, **45**, 1733.
42 G. Gorrasi, M. Tortora, V. Vittoria, G. Galli and E. Chiellini, *J. Polym. Sci., Part B: Polym. Lett.*, 2002, **40**, 1118.
43 H.-C. Lee, T.-W. Lee, Y.-T. Lim and O. O. Park, *Appl. Clay Sci.*, 2002, **21**, 287.
44 J. Zhu, F. M. Uhl, A. Morgan and C. A. Wilkie, *Chem. Mater.*, 2001, **13**, 4649.
45 X. Zheng and C. A. Wilkie, *Polym. Degrad. Stab.*, 2003, **81**, 539.
46 S. Bourbigot, E. Devaux and X. Flambard, *Polym. Degrad. Stab.*, 2002, **75**, 297.
47 F. Belluci, G. Camino, A. Flache and A. Sarra, *Polym. Degrad. Stab.*, 2007, **92**, 425.
48 P. Aranda and E. Ruiz-Hitzky, *Chem. Mater.*, 1992, **4**, 1395.
49 E. Ruiz-Hitzky and P. Aranda, *Adv. Mater.*, 1990, **2**, 545.
50 W. Jia, E. Segal, D. Kornemandel, Y. Lamhot, M. Narkis and A. Siegmann, *Synth. Met.*, 2002, **128**, 115.
51 D. Schmidt, D. Shah and E. P. Giannelis, *Curr. Opin. Solid State Mater. Chem.*, 2002, **6**, 205.
52 S. S. Ray, K. Yamada, M. Okamoto, Y. Fujimoto, A. Ogami and K. Ueda, *Polymer*, 2003, **44**, 6633.
53 M. Darder, A. I. Ruiz, P. Aranda, H. Van Damme and E. Ruiz-Hitzky, *Curr. Nanosci.*, 2006, **2**, 231.
54 J. W. Rhim, S. I. Hong, H. M. Park and P. K. W. Ng, *J. Agric. Food Chem.*, 2006, **54**, 5814.
55 K. Haraguchi, T. Takehisa and M. Ebato, *Biomacromolecules*, 2006, **7**, 3267.
56 Y. C. Dong and S. S. Feng, *Biomaterials*, 2005, **26**, 6068.
57 R. Y. Lochhead, C. T. Haynes, S. R. Jones and V. Smith, *Appl. Surf. Sci.*, 2006, **252**, 2535; L. Cabedo, J. L. Feijoo, M. P. Villanueva, J. M. Lagaron and E. Gimenez, *Macromol. Symp.*, 2006, **233**, 191.
58 R. A. Schoonheydt, T. J. Pinnavaia, G. Lagaly and N. Gangas, *Pure Appl. Chem.*, 1999, **71**, 2367.
59 R. E. Grim, *Applied Clay Mineralogy*, McGraw-Hill Book Company, New York, 1962.
60 R. E. Grim, *Clay Mineralogy*, 2nd edn., McGraw-Hill Book Company, New York, 1968.
61 B. K. G. Theng, *Formation and properties of clay-polymer complexes*, Elsevier Scientific Publishing Company, Amsterdam, 1979, p. 37–70.
62 T. J. Pinnavaia, *Science*, 1983, **220**, 365.
63 A. K. Helmy, E. A. Ferreiro and S. G. D. Bussetti, *J. Colloid Interface Sci.*, 1999, **210**, 167.
64 B. Chen and J. R. G. Evans, *J. Phys. Chem. B*, 2004, **108**, 14986.
65 E. P. Giannelis, *JOM -J. Min. Met. Mat. S.*, 1992, **44**, 28.
66 B. Chen and J. R. G. Evans, *Philos. Mag.*, 2005, **85**, 1519.
67 T. Stumpf, A. Bauer, F. Coppin and J. I. Kim, *Environ. Sci. Technol.*, 2001, **35**, 3691.
68 D. M. Nevskaia, A. Guerrero-Ruiz and J. D. D. Lopez-Gonzalez, *J. Colloid Interface Sci.*, 1996, **181**, 571.
69 T. Kyu, G. C. Zhu, Z. L. Zhou, Y. Tajuddin and S. Qutubuddin, *J. Polym. Sci., Part B: Polym. Lett.*, 1996, **34**, 1769.
70 B. K. G. Theng, *Chemistry of clay-organic reactions*. Adam Hilger, London. 1974, pp. 17–31, 54.
71 J. E. Gardolinski, L. C. M. Carrera, M. P. Cantao and F. Wypych, *J. Mater. Sci.*, 2000, **35**, 3113.
72 R. A. Vaia, K. D. Jandt, E. J. Kramer and E. P. Giannelis, *Chem. Mater.*, 1996, **8**, 2628.
73 M. S. Stul and L. V. Leemput, *Surf. Technol.*, 1981, **16**, 89; K. W. Weissmahr, M. Hildenbrand, R. P. Schwarzenbach and S. B. Haderlein, *Environ. Sci. Technol.*, 1999, **33**, 2593.
74 H. C. Greenwell, A. A. Bowden, B. Chen, P. Boulet, J. R. G. Evans, P. V. Coveney and A. Whiting, *J. Mater. Chem.*, 2006, **16**, 1082.
75 P. Maiti and M. Okamoto, *Macromol. Mater. Eng.*, 2003, **288**, 440.
76 J. Zhang and C. A. Wilkie, *Polym. Degrad. Stab.*, 2004, **83**, 301.
77 D. Wang and C. A. Wilkie, *Polym. Degrad. Stab.*, 2003, **82**, 309.
78 S. Su, D. D. Jiang and C. A. Wilkie, *Polym. Degrad. Stab.*, 2004, **83**, 321.
79 X. Zheng and C. A. Wilkie, *Polym. Degrad. Stab.*, 2003, **82**, 441.
80 A.-Y. A. Shin, L. C. Simon, J. B. P. Soares and G. Scholz, *Polymer*, 2003, **44**, 5317.
81 O. Yoshida and M. Okamoto, *Macromol. Rapid Commun.*, 2006, **27**, 751.
82 T. Saito, M. Okamoto, R. Hiroi, M. Yamamodo and T. Shiroi, *Macromol. Mater. Eng.*, 2006, **291**, 1367.
83 T. Saito, M. Okamoto, R. Hiroi, M. Yamamodo and T. Shiroi, *Polymer*, 2007, **48**, 4143.
84 J. Zhang, D. D. Jiang and C. A. Wilkie, *Polym. Degrad. Stab.*, 2006, **91**, 641.
85 C. B. Hedley, G. Yuan and B. K. G. Theng, *Appl. Clay Sci.*, 2007, **35**, 180.
86 M. Chen, B. Chen and J. R. G. Evans, *Nanotechnology*, 2005, **16**, 2334.
87 G. Harikrishnan, T. U. Patro and D. V. Khakhar, *Ind. Eng. Chem. Res.*, 2006, **45**, 7126.
88 P. M. Ajayan, O. Stephan, C. Colliex and D. Trauth, *Science*, 1994, **265**, 1212.
89 J. N. Coleman, U. Khan, W. J. Blau and Y. K. Gun'ko, *Carbon*, 2006, **44**, 1624.
90 A. Bakandritsos, A. Simopoulos and D. Petridis, *Chem. Mater.*, 2005, **17**, 3468.

91 S. Peeterbroeck, M. Alexandre, J. B. Nagy, N. Moreau, A. Destree, F. Monteverde, A. Rulmont, R. Jerome and P. Dubois, *Macromol. Symp.*, 2005, **221**, 115.
92 P. Boulet, A. A. Bowden, P. V. Coveney and A. Whiting, *J. Mater. Chem.*, 2003, **13**, 2540.
93 B. Chen, A. A. Bowden, H. C. Greenwell, P. Boulet, P. V. Coveney, A. Whiting and J. R. G. Evans, *J. Polym. Sci., Part B: Polym. Lett.*, 2005, **43**, 1785.
94 B. Chen and J. R. G. Evans, *Polym. Int.*, 2005, **54**, 807.
95 C. Y. Wan, Y. Zhang, Y. X. Zhang, X. Y. Qiao and G. M. Teng, *J. Polym. Sci., Part B: Polym. Lett.*, 2004, **42**, 286.
96 R. A. Vaia, H. Ishii and E. P. Giannelis, *Chem. Mater.*, 1993, **5**, 1694.
97 C. Zeng and L. J. Lee, *Macromolecules*, 2001, **34**, 4098.
98 X. Huang, S. Lewis, W. J. Brittain and R. A. Vaia, *Macromolecules*, 2000, **33**, 2000.
99 T. Lan, P. D. Kaviratna and T. J. Pinnavaia, *J. Phys. Chem. Solids*, 1996, **57**, 1005.
100 N. Furuichi, Y. Kurokawa, K. Fujita, A. Oya, H. Yasuda and M. Kiso, *J. Mater. Sci.*, 1996, **31**, 4307.
101 Z. Shen, G. P. Simon and Y.-B. Cheng, *Polymer*, 2002, **43**, 4251.
102 J.-H. Chang, D.-K. Park and K. J. Ihn, *J. Polym. Sci., Part B: Polym. Lett.*, 2001, **39**, 471.
103 B. Bloys, N. Davis, B. Smolen, L. Bailey, O. Houwen, P. Reid, J. Sherwood, L. Fraser and M. Hodder, *Schlumberger Oilfield Rev.*, 1994, **6**, 3; E. S. Boek, P. V. Coveney, B. Craster and P. I. Reid, in *Chemicals in the oil industry: recent developments: proceedings of the sixth international symposium on chemistry in the oil industry*, ed. L. Cookson and P. H. Ogden, Royal Society of Chemistry, Cambridge, 1999; A. S. Bains, E. S. Boek, P. V. Coveney, S. J. Williams and M. V. Akbar, *Mol. Simul.*, 2001, **26**, 101.
104 P. V. Coveney, M. Watkinson, A. Whiting and E. S. Boek, *Stabilizing Clayey Formations*, US Patent Number 6,787,507.
105 M. Kawasumi, N. Hasegawa, M. Kato, A. Usuki and A. Okada, *Macromolecules*, 1997, **30**, 6333.
106 W. Krawiec, L. G. Scanlon, J. P. Fellner, R. A. Vaia, S. Vasudevan and E. P. Giannelis, *J. Power Sources*, 1995, **54**, 310.
107 Q. Zhang, Q. Zax, L. Jiang and Y. Lei, *Polym. Int.*, 2000, **49**, 1561.
108 A. Usuki, A. Tukigase and M. Kato, *Polymer*, 2002, **43**, 2185.
109 F. Gao, S. Chen and J. B. Hull, *J. Mater. Sci. Lett.*, 2001, **20**, 1807.
110 N. Khaorapapong, K. Kuroda, H. Hashizume and M. Ogawa, *Appl. Clay Sci.*, 2001, **19**, 69.
111 J.-M. Sequaris, F. Bassmann, A. Hild, H. D. Narres and M. J. Schwuger, *Colloids Surf., A*, 1999, **159**, 503–512.
112 M. Z. Xu, Y. S. Choi, Y. K. Kim, K. H. Wang and I. J. Chung, *Polymer*, 2003, **44**, 6395.
113 Q. Zhao and E. T. Samulski, *Polymer*, 2006, **47**, 663.
114 H. A. Barnes, J. F. Hutton and K. Walters, *An introduction to rheology*, Elsevier Science B. V., Amsterdam, 1998, pp. 115–139.
115 H. C. Greenwell, W. Jones, P. V. Coveney and S. Stackhouse, *J. Mater. Chem.*, 2006, **16**, 708.
116 P. Boulet, H. C. Greenwell, S. Stackhouse and P. V. Coveney, *THEOCHEM*, 2006, **762**, 33.
117 M. Pelletier, L. J. Michot, B. Humbert, O. Barrès, J.-B. D. de la Caillerie and J.-L. Robert, *Am. Mineral.*, 2003, **88**, 1801.
118 S. Stackhouse, P. V. Coveney and E. Sandré, *J. Am. Chem. Soc.*, 2001, **123**, 11764.
119 A. T. Hagler, E. Huler and S. Lifson, *J. Am. Chem. Soc.*, 1974, **96**, 5319.
120 S. L. Mayo, B. D. Olafson and W. A. Goddard, *J. Phys. Chem.*, 1990, **94**, 8897.
121 R. T. Cygan, J. J. Liang and A. G. Kalinichev, *J. Phys. Chem. B*, 2004, **108**, 1255.
122 B. J. Teppen, K. Rasmussen, P. M. Bertsch, D. M. Miller and L. Schäfer, *J. Phys. Chem. B*, 1997, **101**, 1579.
123 J. L. Suter, P. V. Coveney, H. C. Greenwell and M.-A. Thyveetil, *J. Phys. Chem. C*, 2007, **111**, 8248.
124 V. Causin, C. Marega, A. Marigo and G. Ferrara, *Polymer*, 2005, **46**, 9533.
125 A. Sinsawat, K. L. Anderson, R. A. Vaia and B. L. Farmer, *J. Polym. Sci., Part B: Polym. Lett.*, 2003, **41**, 3272.
126 R. A. Vaia, S. Vasudevan, W. Krawiec and E. P. Giannelis, *Adv. Mater.*, 1995, **7**, 154.
127 D. K. Yang and D. B. Zax, *J. Chem. Phys.*, 1999, **110**, 5325.
128 E. Hackett, E. Manias and E. P. Giannelis, *Chem. Mater.*, 2000, **12**, 2161.
129 J. Bujdák, E. Hackett and E. P. Giannelis, *Chem. Mater.*, 2000, **12**, 2168.
130 V. Kuppa and E. Manias, *Chem. Mater.*, 2002, **14**, 2171.
131 M. X. Reinholdt, R. J. Kirkpatrick and T. J. Pinnavaia, *J. Phys. Chem. B*, 2005, **109**, 16296.
132 M. Pospísil, P. Capková, D. Merínská, Z. Malác and J. Simoník, *J. Colloid Interface Sci.*, 2001, **236**, 127.
133 Q. H. Zeng, A. B. Yu, G. Q. Lu and R. K. Standish, *Chem. Mater.*, 2003, **15**, 4732.
134 Q. H. Zeng, A. B. Yu, G. Q. Lu and R. K. Standish, *J. Phys. Chem. B*, 2004, **108**, 10025.
135 H. Heinz, H. J. Castelijns and U. W. Suter, *J. Am. Chem. Soc.*, 2003, **125**, 9500.
136 H. Heinz and U. W. Suter, *J. Phys. Chem. B*, 2004, **108**, 18341.
137 M. Pospísil, A. Kalendová, P. Capková, J. Simoník and M. Valásková, *J. Colloid Interface Sci.*, 2004, **277**, 154.
138 D. R. Paul, Q. H. Zeng, A. B. Yu and G. Q. Lu, *J. Colloid Interface Sci.*, 2005, **292**, 462.
139 B. Minisini and F. Tsobnang, *Composites, Part A*, 2005, **36**, 539.
140 G. Tanaka and L. A. Goettler, *Polymer*, 2002, **43**, 541.
141 M. Fermeglia, M. Ferrone and S. Pricl, *Fluid Phase Equilib.*, 2003, **212**, 315.
142 R. Toth, A. Coslanich, M. Ferrone, M. Fermeglia, S. Pricl, S. Miertus and E. Chiellini, *Polymer*, 2004, **45**, 8075.
143 D. Sikdar, D. R. Katti and K. S. Katti, *Langmuir*, 2006, **22**, 7738.
144 K. S. Katti, D. Sikdar, D. R. Katti, P. Ghosh and D. Verma, *Polymer*, 2006, **47**, 403.
145 D. Sikdar, D. R. Katti, K. S. Katti and R. Bhowmik, *Polymer*, 2006, **47**, 5196.
146 F. Gardebien, A. Gaudel-Siri, J. L. Bredas and R. Lazzaroni, *J. Phys. Chem. B*, 2004, **108**, 10678.
147 D. Aleperstein, N. Artzi, A. Siegmann and M. Narkis, *J. Appl. Polym. Sci.*, 2005, **97**, 2060.
148 V. Kuppa, T. M. D. Foley and E. Manias, *Eur. Phys. J. E*, 2003, **12**, 159.
149 V. Kuppa and E. Manias, *J. Polym. Sci., Part B: Polym. Lett.*, 2005, **43**, 3460.
150 H. C. Greenwell, M. J. Harvey, P. Boulet, A. A. Bowden, P. V. Coveney and A. Whiting, *Macromolecules*, 2005, **38**, 6189.
151 P. V. Coveney, J. L. W. Griffin, M. Watkinson, A. Whiting and E. Boek, *Mol. Simul.*, 2002, **28**, 295.
152 P. Boulet, P. V. Coveney and S. Stackhouse, *Chem. Phys. Lett.*, 2004, **389**, 261.
153 A. Gaudel-Siri, P. Brocorens, D. Siri, F. Gardebien, J.-L. Brédas and R. Lazzaroni, *Langmuir*, 2003, **19**, 8287.
154 E. Fois, A. Gamba and A. Tilocca, *Microporous Mesoporous Mater.*, 2003, **57**, 263.
155 A. J. A. Aquino, D. Tunega, G. Haberhauer, M. H. Gerzabek and H. Lischka, *J. Comput. Chem.*, 2003, **24**, 1853.
156 A. J. A. Aquino, D. Tunega, M. H. Gerzabek and H. Lischka, *J. Phys. Chem. B*, 2004, **108**, 10120.
157 H. C. Greenwell, S. Stackhouse, P. V. Coveney and W. Jones, *J. Phys. Chem. B*, 2003, **107**, 3476.
158 O. L. Manevitch and G. C. Rutledge, *J. Phys. Chem. B*, 2004, **108**, 1428.
159 D. R. Katti, P. Ghosh, S. Schmidt and K. S. Katti, *Biomacromolecules*, 2005, **6**, 3276.
160 M. Zabat, M. Vayer-Besancon, R. Harba, S. Bonnamy and H. Van Damme, *Prog. Colloid Polym. Sci.*, 1997, **105**, 96.
161 M.-A. Thyveetil, P. V. Coveney, J. L. Suter and H. C. Greenwell, *Chem. Mater.*, 2007, **19**, 5510.
162 N. Sheng, M. C. Boyce, D. M. Parks, G. C. Rutledge, J. I. Abes and R. E. Cohen, *Polymer*, 2004, **45**, 487.
163 L. J. Zhu and K. A. Narh, *J. Polym. Sci., Part B: Polym. Lett.*, 2004, **42**, 2391.
164 V. A. Buryachenko, A. Roy, K. Lafdi, K. L. Anderson and S. Chellapilla, *Compos. Sci. Technol.*, 2005, **65**, 2435; O. Borodin, D. Bedrov, G. D. Smith, J. Nairn and S. Bardenhagen, *J. Polym. Sci., Part B: Polym. Lett.*, 2005, **43**, 1005; P. K. Valavala and G. M. Odegard, *Rev. Adv. Mater. Sci.*, 2005, **9**, 34; O. Borodin,

D. Bedrov, G. D. Smith, J. Nairn and S. Bardenhagen, *J. Polym. Sci., Part B: Polym. Lett.*, 2005, **43**, 1005; P. K. Valavala and G. M. Odegard, *Rev. Adv. Mater. Sci.*, 2005, **9**, 34.
165 V. V. Ginzburg and A. C. Balazs, *Macromolecules*, 1999, **32**, 5681.
166 J. S. Smith, D. Bedrov and G. D. Smith, *Compos. Sci. Technol.*, 2005, **63**, 1599.
167 K. L. Anderson, A. Sinsawat, R. A. Vaia and B. L. Farmer, *J. Polym. Sci., Part B: Polym. Lett.*, 2005, **43**, 1014.
168 R. Jenkins and R. L. Snyder, *Introduction to X-ray powder diffractometry*, Wiley, Chichester, 1996, pp. 195–200.
169 T. D. Fornes, P. J. Yoon, H. Keskkula and D. R. Paul, *Polymer*, 2001, **42**, 9929.
170 S. Bourbigot, D. L. VanderHart, J. W. Gilman, W. H. Awad, R. D. Davis, A. B. Morgan and C. A. Wilkie, *J. Polym. Sci., Part B: Polym. Lett.*, 2003, **41**, 3188.
171 A. Vermogen, K. Masenelli-Varlot, R. Seguela, J. Duchet-Rumeau, S. Boucard and P. Prele, *Macromolecules*, 2005, **38**, 9661.
172 J. Zhao, A. B. Morgan and J. D. Harris, *Polymer*, 2005, **23**, 8641.
173 E. Ferrage, F. Martin, A. Boudet, S. Petit, G. Fourty, F. Jouffret, P. Micoud, P. de Parseval, S. Salvi, C. Bourgerette, J. Ferret, Y. Saint-Gerard, S. Buratto and J. P. Fortune, *J. Mater. Sci.*, 2002, **37**, 1561.
174 G. B. A. Lim and D. R. Lloyd, *Polym. Eng. Sci.*, 1993, **33**, 513.
175 R. A. Vaia and E. P. Giannelis, *Macromolecules*, 1997, **30**, 7990.
176 Z. Shen, G. P. Simon and Y.-B. Cheng, *Eur. Polym. J.*, 2003, **39**, 1917.
177 R. L. Parfitt and D. J. Greenland, *Clay Miner.*, 1970, **8**, 305.
178 X. Fu and X. Qutubuddin, *Polymer*, 2001, **42**, 807.
179 R. Ullman, *Encyclopaedia of polymer technology*, vol. 1, ed. H. F. Mark, N. G. Gaylord and N. M. Bikales , Interscience, New York, 1964, p. 551–567.
180 A. Nelson and T. Cosgrove, *Langmuir*, 2004, **20**, 2298.
181 E. J. Acosta, Y. Deng, G. N. White, J. B. Dixon, K. J. McInnes, S. A. Senseman, A. S. Frantzen and E. E. Simanek, *Chem. Mater.*, 2003, **15**, 2903.
182 E. P. Giannelis, R. Krishnamoorti and E. Manias, *Adv. Polym. Sci.*, 1999, **138**, 107.
183 D. Gersappe, *Phys. Rev. Lett.*, 2002, **89**, 058301–1.
184 K. Wang, S. Liang, J. Deng, H. Yang, Q. Zhang, Q. Fu, X. Dong, D. Wang and C. C. Han, *Polymer*, 2006, **47**, 7131.
185 W. Zhong, X. Qiao, K. Sun, G. Zhang and X. Chen, *J. Appl. Polym. Sci.*, 2006, **99**, 1523.
186 Y. S. Thio, A. S. Argon, R. E. Cohen and M. Weinberg, *Polymer*, 2002, **43**, 3661.
187 D. Fragiadakis, P. Pissis and L. Bokobza, *Polymer*, 2005, **46**, 6001.
188 Y. Miwa, A. R. Drews and S. Schlick, *Macromolecules*, 2006, **39**, 3304.
189 S. Granick and H. W. Hu, *Langmuir*, 1994, **10**, 3857; J. Peanasky, L. L. Cai, S. Granick and C. R. Kessel, *Langmuir*, 1994, **10**, 3874; P. Sens, C. M. Marques and J. F. Joanny, *Macromolecules*, 1994, **27**, 3812.
190 J. C. Israelachvili, *Intermolecular and surface forces*. 2nd edn, Academic Press, London, 1998, pp. 291–293.
191 J. W. Cho and D. R. Paul, *Polymer*, 2001, **42**, 1083.
192 I. Cendoya, D. Lopez, A. Alegria and C. Mijangos, *J. Polym. Sci., Part B: Polym. Lett.*, 2001, **39**, 1968.
193 M. A. Kader, K. Kim, Y. S. Lee and C. Nah, *J. Mater. Sci.*, 2006, **41**, 7341.
194 X. L. Xie, Q. X. Liu, R. K. Y. Li, X. P. Zhou, Q. X. Zhang, Z. Z. Yu and Y. W. Mai, *Polymer*, 2004, **45**, 6665.
195 A. Bansal, H. C. Yang, C. Z. Lu, K. W. Cho, B. C. Benicewicz, S. K. Kumar and L. S. Schadler, *Nat. Mater.*, 2005, **4**, 693.
196 B. Chen and J. R. G. Evans, *Macromolecules*, 2006, **39**, 1790.
197 B. Chen and J. R. G. Evans, *Scr. Mater.*, 2006, **54**, 1581.
198 R. M. Christensen, *Mechanics of composite materials*, John Wiley & Sons, New York, 1979; pp. 46–48, 100–144; R. M. Christensen, *J. Eng. Mater. Technol.*, 1979, **101**, 299.
199 J. C. Halpin, *Primer on composite materials: analysis*, Technomic Publishing Co., Inc, Pennsylvania, 1984, p 130–140.
200 Z. Hashin and S. Shtrikman, *J. Mech. Phys. Solids*, 1963, **11**, 127.
201 L. J. Gibson and M. F. Ashby, *Cellular solids: structure and properties*, 2nd edn, Cambridge University Press, Cambridge, 1997, p 36.
202 H. X. Peng, Z. Fan and J. R. G. Evans, *Mater. Sci. Eng., A*, 2001, **303**, 37; M. Zhao, G. H. Wu, Z. Dou and L. T. Zhang, *Mater. Sci. Eng., A*, 2004, **374**, 303.
203 Y. Benveniste, *Mech. Mater.*, 1987, **6**, 147.
204 R. M. Christensen, *J. Mech. Phys. Solids*, 1990, **38**, 379.
205 G. Lielens, P. Pirotte, A. Couniot, F. Dupret and R. Keunings, *Composites, Part A*, 1998, **29**, 63.
206 C. L. Tucker and E. Liang, *Compos. Sci. Technol.*, 1999, **59**, 655.
207 P. V. Coveney, R. S. Saksena, S. J. Zasada, M. McKeown and S. Pickles, *Comput. Phys. Commun.*, 2007, **176**, 406.
208 J. Q. Broughton, F. F. Abraham, N. Bernstein and E. Kaxiras, *Phys. Rev. B: Condens. Matter Mater. Phys.*, 1999, **60**, 2391.
209 G. De Fabritiis, R. Delgado-Buscalioni and P. V. Coveney, *Phys. Rev. Lett.*, 2006, **97**, 134501.
210 *Scientific grid computing*, theme issue of *Philos. Trans. R. Soc. London, Ser. A.*, ed. P. V. Coveney, 2005, **363**, 1701–2095.

